Title
ZFP36-Mediated mRNA Decay Regulates Metabolism Downstream of Growth Factor Signaling

Author
Cicchetto, Andrew Charles

Publication Date
2022

Peer reviewed|Thesis/dissertation

UNIVERSITY OF CALIFORNIA

Los Angeles

ZFP36-Mediated mRNA Decay Regulates Metabolism Downstream of Growth Factor Signaling

A dissertation submitted in partial satisfaction of the

requirements for the degree Doctor of Philosophy

in Molecular and Medical Pharmacology

by

Andrew Charles Cicchetto

2022

ABSTRACT OF THE DISSERTATION

ZFP36-Mediated mRNA Decay Regulates Metabolism

Downstream of Growth Factor Signaling

by

Andrew Charles Cicchetto

Doctor of Philosophy in Molecular and Medical Pharmacology

University of California, Los Angeles, 2022

Professor David A. Nathanson, Co-Chair

Professor Heather R. Christofk, Co-Chair

Cellular metabolism is tightly regulated by growth factor signaling, which promotes metabolic rewiring to support growth and proliferation. While growth factor-induced transcriptional and post-translational modes of metabolic regulation have been well-defined, whether post-transcriptional mechanisms impacting mRNA stability regulate this process is less clear. Here, we present the ZFP36/L1/L2 family of RNA-binding proteins and mRNA decay factors as key drivers of metabolic regulation downstream of acute growth factor signaling. We quantitatively catalogue metabolic enzyme and nutrient transporter mRNAs directly bound by ZFP36 following growth factor stimulation – many of which encode rate-limiting steps in metabolic pathways. Further, we show that ZFP36 directly promotes the mRNA decay of Enolase 2 (Eno2), altering Eno2 protein expression and enzymatic activity, and provide evidence of a ZFP36/Eno2 axis during VEGF-stimulated developmental retinal angiogenesis. Thus, ZFP36-mediated mRNA decay serves as

an important mode of metabolic regulation downstream of growth factor signaling within dynamic cell and tissue states.

The dissertation of Andrew Charles Cicchetto is approved.

Hilary Ann Coller

Thomas Aguiar Vallim

David A. Nathanson, Committee Co-Chair

Heather R. Christofk, Committee Co-Chair

University of California, Los Angeles

2022

DEDICATION

For my Grandpa – Charles Richard Barnard

TABLE OF CONTENTS

LIST OF FIGURES AND TABLES

ACKNOWLEDGEMENTS

This work would not be possible without the support and guidance of all the members of the Christofk Lab. Thank you for your all the productive scientific discussions and mentorship that helped shaped my experience through graduate school. I am grateful for the opportunity to have worked with each of you and am proud of what we have accomplished together!

I would like to acknowledge all my committee members including Thomas Vallim, Hilary Coller, and David Nathanson, for their support and guidance. I feel grateful to have learned from each of you, and have your direction to shape my project over the years.

I would like to acknowledge my parents, Jan and Gary, and my brother, Daniel, for their unconditional love and support. Your encouragement and praise helped me persevere through challenges. The daily support from my mom has been a support beam for me that I relied on for motivation every day!

I would like to thank my wife, Miranda, for her love and support, and our two babies, Emmitt and Grace, who are our everything. Thank you for balancing my days with family time and reminding me to keep everything in perspective.

Lastly, I would like to thank my advisor and mentor, Heather Christofk. Your support over the years has meant so much to me. Thank you for helping me to balance the lab with my family. You have been a role model for me both personally and professionally, and I am grateful for everything you have taught me.

The research presented in this dissertation was performed under the direction of Heather R. Christofk, supported by the UCLA Vascular Biology Training Grant awarded to A.C.C., and is a version of the following unpublished work submitted for peer review:

Cicchetto A, Jacobson E, Sunshine H, Wilde B, Krall A, Jarrett K, Sedgeman L, Turner M, Plath K, Arispe L, Vallim T, Christofk H. ZFP36-mediated mRNA decay regulates metabolism downstream of growth factor signaling. (Submitted).

VITA

EDUCATION –

Master of Arts (M.A.), Stem Cell Research, California State University, Sacramento, 2014 to 2016.

Bachelor of Science (B.S.), Biomedical Sciences, California State University, Sacramento, 2011 to 2013.

PUBLICATIONS –

Cicchetto A, Jacobson E, Sunshine H, Wilde B, Krall A, Jarrett K, Sedgeman L, Turner M, Plath K, Iruela-Arispe L, Vallim T, Christofk H. ZFP36-Mediated mRNA Decay Regulates Metabolism Downstream of Growth Factor Signaling. (under review).

Hodson A, **Cicchetto A**, and Fierro F. Real time PCR assays to detect and quantify the nematodes Pratylenchus vulnus and Mesocriconema xenoplax. *Crop Protection* (2021).

Albrecht L, Tejeda-Muñoz N, Bui M, **Cicchetto A**, DiBiagioD, Colozza G, Schmid E, Piccolo S, Christofk H and De Robertis E. GSK3 Inhibits Macropinocytosis and Lysosomal Activity through the Wnt Destruction Complex Machinery. *Cell Reports* (2020).

Clark K, Fierro F, Ko E, Walker N, Arzi B, Tepper C, Dahlenburg H, **Cicchetto A**, Kol A, Marsh L, Murphy W, Fazel N, Borjesson D. Human and Feline Adipose Derived Mesenchymal Stem Cells have comparable phenotype, immunomodulatory functions and transcriptome. *Stem Cell Research & Therapy* (2017).

Kalomoiris S, **Cicchetto A**, Lakatos K, Nolta J, Fierro F. FGF2 Regulates High Mobility Group A2 Expression in Human Bone Marrow-Derived Mesenchymal Stem Cells. *Journal of Cellular Biochemistry* (2016).

HONORS, AWARDS & EXTRACURRICULAR ACTIVITIES –

NIH T32 Vascular Biology Training Grant (5T32HL069766), UCLA, 2019 to 2022.

Trainee Innovation Award, Department of Biological Chemistry, UCLA, 2021.

Clinical and Translational Science Institute (CTSI) Core Voucher Award, UCLA, 2020.

Student Representative of the Department of Molecular and Medical Pharmacology, UCLA, 2019 to 2020.

Cross-Disciplinary Scholars in Science and Technology (CSST) Undergraduate Mentorship Program, UCLA, 2018.

Chapter 1

Introduction: Growth Factor Signaling and the ZFP36 Family of RNA-Binding Proteins

Presented within this dissertation is a framework for how cells quickly respond to growth factor signaling through coordinated processes converging gene expression programs and metabolic reprogramming with cell growth. Cells are highly sensitive to external stimuli and reserve multiple mechanisms to facilitate phenotypic outcomes. These mechanisms often exist within cell type- or tissue-specific constraints dictated by the local environment or homeostatic requirements at the organismal level[1,2]. Highly conserved signaling pathways mediate cellular responses in cooperation with downstream gene expression programs[3,4]. The degree to which cell behavior changes is determined by the relative summation of these variables, and its dysregulation can lead to diseases such as cancer[5]. Existing evidence outlined below will highlight key aspects of the abovementioned biological phenomena including current gaps in knowledge and rationale for further investigation. Next, proposed hypotheses addressed through experimental means and presented within subsequent chapters of this dissertation will be listed. Lastly, the chapter will conclude with a brief summary of our findings.

Growth factor signaling-induced gene expression intersects with changes in metabolism

Cell responses to growth factor signaling engages highly dynamic gene expression circuits to facilitate nutrient acquisition and anabolism. Growth factor inputs act on a cell and signal-specific basis as well as at the level of signal dose and duration with respect to receptor engagement[6]. Recent advances in gene expression modeling algorithms attempt to identify patterns within these complex networks producing various regulatory motifs including negative and positive feedback loops, oscillating trajectories, and AND/OR gate logic[6,7]. The current interest to pursue a deeper understanding of gene expression modules with constituent-specific resolution is clear- harnessing control of such systems may give rise to novel therapeutic approaches for treating aberrant signaling activation as is the case during malignant transformation[8].

One important family of genes that are classified according to their kinetic expression profile is the ZFP36, ZFP36L1, and ZFP36L2 family of RNA-binding proteins and mRNA decay factors. These proteins are considered immediate early genes (IEGs) owing to their ability to be transcriptionally activated downstream of MAPK (ERK, p38, JNK) signaling within minutes in the absence of *de novo* protein expression[9]. Signaling-activated transcription factors including ELK and EGR are among the most well-described mediators of ZFP36 family member activation[10]. Once turned on, ZFP36 proteins regulate gene expression post-transcriptionally by directly binding AU-rich elements in the 3'UTR of target transcripts and promoting their mRNA decay in cooperation with CCR4-CAF1-NOT1 deadenylase machinery[11]. The broad repertoire of ZFP36/L1/L2 target transcripts are generally thought to be part of the acute growth factor signaling gene expression modules themselves, including other IEGs such as dual specificity phosphatases (DUSPs), AP-1 complex members (c-fos and c-jun) and c-Myc among others[12]. This activity places them within a growth-suppressive negative feedback loop with upstream signaling activation. Indeed, ZFP36 family member loss is selected for in various cancers[13]. However, whether this is due to a direct rise in ARE-containing ZFP36/L1/L2 target genes – of which nearly 10% of the eukaryotic transcriptome contains[14] – or a result of the indirect outputs of their target genes' transcriptional activity remains unclear.

Also found within acute growth factor signaling gene expression clusters are metabolic genes. These mRNAs encode nutrient transporter adapter proteins, solute carriers and metabolic enzymes – some of which indeed contain AREs[12]. Although metabolic reprogramming is a hallmark of growth factor signaling, most studies have assigned posttranslational mechanisms, subcellular localization dynamics and transcriptional regulation of metabolic enzymes and nutrient transporters as the primary means of achieving such changes[15]. Given that ZFP36-mediated mRNA decay activity participates among these various levels of regulation on the same timescale, it is plausible that post-transcriptional metabolic regulation is an underappreciated, yet key, cell

response mechanism[16]. Further investigations are needed to deepen and broaden our understanding of how ZFP36 proteins regulate metabolism the level of mRNA decay.

Here, we seek to explore the intersection of growth factor signaling with mRNA-decay-mediated metabolic rewiring. We hypothesize that ZFP36 family member-mediated mRNA decay orchestrates this by harnessing a conserved post-transcriptional regulon consisting of metabolic enzymes and nutrient transporters.

Hypotheses addressed within this dissertation –

1. ZFP36 family member expression is regulated by growth factor signaling.

2. ZFP36 regulates metabolic gene expression through direct mRNA decay.

3. ZFP36 proteins regulate metabolism.

Given that growth factor signaling engages ZFP36 family member expression and decay activity while also driving metabolic reprogramming, we seek to build a causal relationship between these two observations. Evidence suggests that metabolism is highly dynamic during acute growth factor signaling, requiring some metabolic genes to be quickly turned off. Conversely, metabolic transcripts upregulated upon acute growth factor signaling require attenuation to avoid aberrant overexpression. We investigate ZFP36-mediated mRNA decay as a way to speed the cellular response thereby coordinating rapid metabolic gene expression switches.

Subsequent evidence provided within this dissertation surveys expression of the ZFP36 family of mRNA-binding proteins downstream of acute growth factor signaling across a variety of cell types

and growth factor stimuli. Through genetic and biochemical means, we quantitatively catalogue metabolic enzyme and nutrient transporter mRNAs directly bound by ZFP36 following growth factor stimulation – many of which encode rate-limiting steps in metabolic pathways. We explore the dependence of these identified metabolic transcripts on ZFP36-mediated mRNA decay and rationally pick one ZFP36 target gene, the glycolytic enzyme Enolase 2, to prove its regulation through a direct mRNA decay mechanism. Further, we provide physiological relevance for this regulation in an *in vivo* model of angiogenesis that is driven by growth factor signaling. Thus, we raise ZFP36-mediated mRNA decay as an important mode of metabolic regulation downstream of growth factor signaling within dynamic cell and tissue states.

REFERENCES

1 Adelaja, A. *et al.* Six distinct NFkappaB signaling codons convey discrete information to distinguish stimuli and enable appropriate macrophage responses. *Immunity* **54**, 916-930 e917, doi:10.1016/j.immuni.2021.04.011 (2021).

2 Lee, H. J. *et al.* Proteomic and Metabolomic Characterization of a Mammalian Cellular Transition from Quiescence to Proliferation. *Cell Rep* **20**, 721-736, doi:10.1016/j.celrep.2017.06.074 (2017).

3 Manning, B. D. & Cantley, L. C. AKT/PKB signaling: navigating downstream. *Cell* **129**, 1261-1274, doi:10.1016/j.cell.2007.06.009 (2007).

4 Manning, B. D. & Toker, A. AKT/PKB Signaling: Navigating the Network. *Cell* **169**, 381-405, doi:10.1016/j.cell.2017.04.001 (2017).

5 Liu, G. Y. & Sabatini, D. M. mTOR at the nexus of nutrition, growth, ageing and disease. *Nat Rev Mol Cell Biol* **21**, 183-203, doi:10.1038/s41580-019-0199-y (2020).

6 Sen, S., Cheng, Z., Sheu, K. M., Chen, Y. H. & Hoffmann, A. Gene Regulatory Strategies that Decode the Duration of NFkappaB Dynamics Contribute to LPS- versus TNF-Specific Gene Expression. *Cell Syst* **10**, 169-182 e165, doi:10.1016/j.cels.2019.12.004 (2020).

7 Tang, Y. & Hoffmann, A. Quantifying information of intracellular signaling: progress with machine learning. *Rep Prog Phys* **85**, doi:10.1088/1361-6633/ac7a4a (2022).

8 Hodson, D. J. *et al.* Deletion of the RNA-binding proteins ZFP36L1 and ZFP36L2 leads to perturbed thymic development and T lymphoblastic leukemia. *Nat Immunol* **11**, 717-724, doi:10.1038/ni.1901 (2010).

9 Brooks, S. A. & Blackshear, P. J. Tristetraprolin (TTP): interactions with mRNA and proteins, and current thoughts on mechanisms of action. *Biochim Biophys Acta* **1829**, 666-679, doi:10.1016/j.bbagrm.2013.02.003 (2013).

10 Florkowska, M. *et al.* EGF activates TTP expression by activation of ELK-1 and EGR-1 transcription factors. *BMC Mol Biol* **13**, 8, doi:10.1186/1471-2199-13-8 (2012).

11 Fu, M. & Blackshear, P. J. RNA-binding proteins in immune regulation: a focus on CCCH zinc finger proteins. *Nat Rev Immunol* **17**, 130-143, doi:10.1038/nri.2016.129 (2017).

12 Amit, I. *et al.* A module of negative feedback regulators defines growth factor signaling. *Nat Genet* **39**, 503-512, doi:10.1038/ng1987 (2007).

13 Rounbehler, R. J. *et al.* Tristetraprolin impairs myc-induced lymphoma and abolishes the malignant state. *Cell* **150**, 563-574, doi:10.1016/j.cell.2012.06.033 (2012).

14 Barreau, C., Paillard, L. & Osborne, H. B. AU-rich elements and associated factors: are there unifying principles? *Nucleic Acids Res* **33**, 7138-7150, doi:10.1093/nar/gki1012 (2005).

15 Waldhart, A. N. *et al.* Phosphorylation of TXNIP by AKT Mediates Acute Influx of Glucose in Response to Insulin. *Cell Rep* **19**, 2005-2013, doi:10.1016/j.celrep.2017.05.041 (2017).

16 Sullivan, W. J. *et al.* Extracellular Matrix Remodeling Regulates Glucose Metabolism through TXNIP Destabilization. *Cell* **175**, 117-132 e121, doi:10.1016/j.cell.2018.08.017 (2018).

CHAPTER 2

ZFP36 Family Member Expression is Regulated by Growth Factor Signaling

INTRODUCTION

Growth factor signaling rapidly induces temporally-defined waves of transcription to reshape the mRNA landscape[1]. Changes can consist of rapid downregulation or upregulation of key gene clusters. Gene signatures that persist after the growth signaling event are likely required for the desired cell state while short-lived changes may participate in regulatory feedback circuits that drive the cellular transition[2]. Interest in deconvoluting these gene expression programs on a context-specific basis has been aided with the development of algorithms that seek to identify logic in the gene constituents and expression profiles[3-5]. Nonetheless, decoding these response programs on a gene-by-gene basis is only beginning to be undertaken.

The ZFP36 family of mRNA-binding proteins and decay factors are within these conserved early gene expression signatures invoked by growth factor signaling[6]. Their expression and decay activity peak within minutes to hours following a growth signaling event[7,8]. The transient nature of their activity is thought to attenuate the induction or accelerate the downregulation of signaling-responsive mRNAs. Importantly, ZFP36 activity is likely a context-specific occurrence dictated by stimulus, cell type, and functional cellular response. For example, many mitogenic growth factor stimuli may induce cell cycle machinery in the early gene expression programs while cytokine-related stimuli may require expression of immune effector molecules[9-11]. In both cases, ZFP36 proteins may be tasked with providing mRNA decay as a means of feedback, interacting with unique target transcripts for each scenario. Dysregulation of these programs through magnitude and duration of ZFP36 expression and decay activity, can alter growth or speed of response times and has relevance to malignant transformation[12].

Here, we profile a variety of growth factor stimuli and cell types to identify an ideal model that is robust in ZFP36 family member activation *in vitro* and *in vivo*. Further, we temporally define the upregulation of ZFP36 family members and dissect the upstream signaling cascades that lead to

expression onset. ZFP36 proteins appear to behave as canonical immediate early genes, being dependent on signaling activated transcription factors without the need for expression of new transcriptional machinery. Therefore, ZFP36 proteins are poised for expression among the dynamic gene sets rapidly and transiently induced by growth factor signaling. This regulation temporally places them within regulatory feedback modules that mediate cell state switching.

RESULTS

To determine the temporality of ZFP36 family member induction in response to growth factor stimulation, we examined the kinetics of Zfp36, Zfp36l1, and Zfp36l2 mRNA expression post-acute exposure of multiple cell lines to various stimuli. We conducted this analysis on a small panel of cultured cell lines – mouse embryonic fibroblasts (MEF), HeLa, A549, MCF-10A, and human foreskin fibroblasts (HFF) – each stimulated with an array of individual growth factors (insulin, IGF-1, bFGF, PDGF-BB, and EGF) at near-physiological concentrations or with serum (FBS), and RNA was harvested at multiple time points post-stimulation (Figure 2-1). We also assessed temporality of ZFP36 induction in the hepatocellular carcinoma (HCC) cell response to serum, bone marrow-derived macrophage (BMDM) response to LPS, and human umbilical vein endothelial cell (HUVEC) response to VEGF (Figure 2-2A). Through our scaled approach, interrogating multiple time points – 30, 60 and 240-minutes – post-stimulation, we captured the dynamic changes in Zfp36 family member mRNA expression during the initial cellular transition from a resting to growing cell state. Further, Zfp36 mRNA in particular appeared to be the most acutely responsive to growth factor signaling, peaking within 30-minutes. A minority of cell lines responded to growth signals by downregulating Zfp36l2 mRNA specifically, as evident in serum-stimulated HFF cells and insulin/IGF-1-stimulated MCF-10A cells. Importantly, not all individual growth factor stimuli induced ZFP36 family member expression across the cell lines tested, perhaps due to the cell line epigenetic and genetic background or display of cognate growth factor receptors on the cell surface. However, serum stimulation increased Zfp36 levels across all cell

lines tested, with MEFs exhibiting the largest dynamic range (Figure 2-1A). The relative potency of serum-induced ZFP36 and ZFP36L1 protein expression was confirmed in MEFs (Figure 2-1B). Consistent with previous reports, rapid and robust induction of ZFP36 and ZFP36L1 protein expression was also observed in livers harvested from mice 15-minutes post-insulin stimulation (Figure 2-2B and 2-2C)[13]. Together, these findings couple growth factor signaling with ZFP36 family member expression on a stimulus- and cell type-specific basis *in vitro* and *in vivo*.

ZFP36 proteins are immediate early genes downstream of MAPK and mTORC1/2 signaling

Given the rapid onset of ZFP36 family member expression in response to growth factor stimulation, we next sought to define the mechanism by which ZFP36 proteins are induced. To this end, we examined how inhibitors of kinases downstream of RTK signaling (MAPK and mTORC1/2) as well as inhibitors of transcription or translation impact ZFP36/L1/L2 induction by serum stimulation. We found that ZFP36/L1/L2 induction is abrogated by MAPK inhibition using a combined Mek and p38 inhibitor cocktail (MAPKi) (Figure 2-3A-D). Torin, a potent and selective mTOR kinase inhibitor, had no effect on Zfp36/l1/l2 mRNA induction in the presence of FBS but reduced protein expression (Figure 2-3E-H). Similarly, blocking translational elongation with cycloheximide (CHX) restricts ZFP36/L1 protein expression without affecting mRNA levels, suggesting a lack of requirement for cofactor expression to facilitate Zfp36 mRNA onset, and that nascent protein synthesis underlies ZFP36 family member expression (Figure 2-3I-L). Interestingly, we observed that CHX alone causes a slight but significant induction of Zfp36 and Zfp36l1 mRNA, though this was not additive with FBS co-treatments, contrary to previously published reports (Figure 2-3J and 2-3K)[13]. Further, a CHX-chase assay revealed that the short half-life of ZFP36L1 protein (<30-minutes) is comparable to that of a well-characterized, inducible transcription factor, c-Myc (Figure 2-3M), suggesting that continuous translation is required to maintain elevated protein expression. Since the transcription inhibitor Actinomycin D blocked ZFP36/L1 protein induction upon FBS stimulation (Figure 2-3N), we postulate the sequence of

events leading to elevated ZFP36 protein is as follows: growth factors activate RTK-MAPK signaling, thereby initiating *de novo* Zfp36 mRNA transcription and translation, where the translation is regulated, at least in part, by mTORC1/2 activity (Figure 2-3O). Collectively, these data are consistent with ZFP36 proteins behaving as immediate early genes.

DISCUSSION

Our study demonstrates that cells and tissues are acutely responsive to growth factor signaling through inducing expression of ZFP36 family members. Upregulation of ZFP36 proteins occurs through signaling dependent mechanisms in the absence of de novo protein synthesis. There is likely a barrier to activation that occurs at the receptor level such that cells *will* respond with ZFP36 family member induction, but this induction is gated by upstream receptors that are present to render the cell sensitive to extracellular communication. Moreover, the magnitude of ZFP36 expression is proportional to the degree of signaling activation. Serum was identified as a universal activator of ZFP36 family member expression likely because serum constituents include multiple growth factor stimuli that simultaneously activate multiple receptors at the cell surface. Therefore, we assert that ZFP36 expression responses are additive such that signaling amplification that occurs through convergent pathways may elicit a larger response; this logic opposes a binary *on/off switch* hypothesis. Given that ZFP36 proteins limit their own expression in a negative feedback look, a saturation point dictated by the relative abundance of Zfp36 mRNA within the transcriptome would likely render it susceptible to autoregulation on a stoichiometric basis among itself and other target mRNA molecules.

ZFP36 expression is dependent on MAPK and mTOR signaling intrinsically integrating nutrient abundance and growth factor signaling status with gene expression. MAPK activation relies on growth factors to switch on circuitry, while mTOR kinase activity requires growth factor signaling *and* nutrients for activation[14]. We show that ZFP36 transcription is induced downstream of MAPK signaling, whereas ZFP36 translation requires mTOR. It would be interesting to test

ZFP36 mRNA upregulation in response to growth factor signaling in the absence of nutrients when mTOR is inactive ie. growth factor signaling in the absence of amino acids. We predict that mRNA upregulation may still occur and represent the terminal point of cellular response to growth signals as it relates to ZFP36 expression. In this scenario, the cell would coordinate its nutrient status with protein synthesis, reserving the ATP-consuming process of protein synthesis to only occur in nutrient favorable environments[15]. This perspective enables ZFP36 induction to also be hinged on the dynamics of nutrient abundance *as much as* it is on the addition of growth factor signaling.

MATERIALS AND METHODS

Mouse experiments

Insulin stimulation:

Wildtype C57BL/6 mice were housed in pathogen-free animal facilities at UCLA in accordance with the UCLA Institutional Animal Care and Use Committee (IACUC). All animal experiments were approved by the UCLA Animal Research Committee (ARC), and were compliant with all relevant ethical regulations. Mice were maintained on a 12-hour light/12-hour dark cycle. On the day of the experiment, mice were fasted for 5-hours, then insulin was dissolved in water and administered (2U/kg) via intraperitoneal (IP) injection; control mice received a water vehicle IP injection only.

MEF cell line generation

MEF isolation:

To prepare mouse embryonic fibroblasts, embryos were obtained through time mating of Zfp36/l1/l2 triple-floxed males and females. Starting at E0.5, pregnant dams were followed with daily weighing until embryonic day E11.5. The dams were euthanized by cervical dislocation following isoflurane induction. Embryos were removed using sterile dissection practices and rinsed in cold PBS. The fetal heads, spinal columns, and organs were removed and the remaining tissue was processed for cell culture. The tissue was dissociated using a razor blade and TrypLE Express (Fisher Cat. # 12604021) and cells were diluted in complete medium (DMEM containing 15% FBS, 10 mM nonessential amino acids, 4 mM L-glutamate, 1 mM sodium pyruvate, and 1% penicillin/streptomycin). Cells from each embryo were pelleted at 300xg for 5 minutes, resuspended in complete medium, and plated in 10 cm tissue culture dishes. Once cells reached ~80% confluency (24-36hr), each MEF cell line was split 1:5. Several plates were cryopreserved, and the remaining cells were used for immortalization.

MEF immortalization:

Zfp36/l1/l2 triple-floxed MEFs were seeded into 6-well dishes at ~75% confluency. The following day, MEFs were exposed to overnight SV40 transfection using Lipofectamine 3000 Reagent (Fisher Cat# L3000001), then medium was replaced with fresh complete medium for an additional 24-hours. Next, MEFs were serial passaged with varying dilutions ranging between 1:3 and 1:10 to ensure survival while applying selective immortalization pressure. Once MEFs were visibly immortal – assessed by nearly 100% adherent cultures without excessive floating/dead cells (~5-10 passages) – they were cryopreserved in 20% FBS-supplemented complete medium with 5% DMSO.

Cell culture conditions

All cell lines, with the exception of MCF-10A cells and HUVECs, were cultured in DMEM containing 1 mM pyruvate and 4 mM glutamine supplemented with 10% fetal bovine serum (FBS) and 1% penicillin/streptomycin in a humidified incubator at 37°C with 5% CO_2 and atmospheric oxygen; MCF-10A cells were cultured in DMEM/F12 supplemented with 5% horse serum, 10µg/mL insulin, 10µg/mL cholera toxin, 500ng/mL hydrocortisone, and 20ng/mL epidermal growth factor (EGF); HUVECs were cultured in MCDB-131-WOFBS (VEC Technologies) with 10% FBS.

Cell culture treatments

Growth factor stimulation:

Stock growth factor solutions were prepared in water in single-use aliquots and applied directly to overnight FBS-deprived cell cultures at approximately 75-85% cell confluency. In the case of 10% FBS treatments, FBS used in standard culture conditions was re-introduced. For experiments involving MCF-10A cells, all culture medium additives were omitted overnight prior to stimulations; 5% horse serum was substituted for 10% FBS.

Inhibitor treatments:

SB2035800 (p38 inhibitor, Selleck Chemical), PD0325901 (MEK1/2 inhibitor, Sigma), Torin (mTOR inhibitor, Tocris Bioscience), cycloheximide (translation inhibitor, Sigma), and actinomycin D (transcription inhibitor, Sigma) were re-suspended in DMSO.

Cell lysis and immunoblotting

Cells were lysed in RIPA buffer supplemented with 2μg/mL aprotinin, 2μg/mL leupeptin, 0.7μg/mL pepstatin, 20mM sodium fluoride, 1mM sodium orthovanadate, 1mM dithiothreitol, 10mM beta-glycerophosphate, and 10mM sodium pyrophosphate. Following protein quantification using Bradford reagent, western blots were performed using standard procedures. The following commercially available antibodies were used for immunoblotting: tristetraprolin (Cell Signaling Technology 71632, 1:500), BRF1/2 (Cell Signaling Technology 2119, 1:1000), ERK (Cell Signaling Technology 9102, 1:1000), phospho-Thr202/Tyr204 ERK (Cell Signaling Technology 4370, 1:1000), S6 kinase (Cell Signaling Technology 2708, 1:1000), phospho-T389 S6 kinase (Cell Signaling Technology 9234, 1:500), c-Myc (Cell Signaling Technology 18583, 1:1000), □-actin (Cell Signaling Technology 3700, 1:1000) and □-tubulin (Sigma T6074, 1:10,000).

Quantitative real-time PCR

Total RNA was isolated from cells using the Qiagen RNeasy Kit followed by on-column DNase digestion and cDNA synthesis using iScript Supermix Kit (Bio-Rad) with 700ng RNA per reaction. Next, cDNA was diluted 5-fold and 2□l was combined with 0.5□M primers in 20□l Power SYBR master mix (Applied Biosystems) and amplified on a QuantStudio5 (Applied Biosystems). Relative transcript levels were calculated using the ΔΔCt method with Rplpo as the reference gene. Table 2-1 provides primer sequences used.

Quantification and statistical analyses

All experiments were carried out in biological triplicate unless otherwise indicated. We performed a two-way ANOVA with Sidak's multiple comparison test to compare Zfp36/l1/l2 mRNA levels by RT-qPCR in response to growth factor stimulation or inhibitor treatments. Bar graphs depict individual data points compared by a two-tailed Student's t test. All significant results were defined as having a p-value < 0.05. Asterisks indicate the significance of the p-value: $*p < 0.05$; $**p < 0.01$; $***p < 0.001$.

Table 2-1: RT-qPCR primers.

Gene	Forward (5'to 3')	Reverse (5'to 3')	species
Zfp36	AACGGAACTCTGCCACAAGT	AGTGGCATCGAGAGCCATAG	mouse
Zfp36l1	TTCACGACACACCAGATCCT	TGAGCATCTTGTTACCCTTGC	mouse
Zfp36l2	TTCTACGATATCGACTTCTTGTGC	AAGCCCGGAGTGAAGCTC	mouse
Rplpo	CACTGGTCTAGGACCCGAGAAG	GGTGCCTCTGGAGATTTTCG	mouse
Zfp36	GACTGAGCTATGTCGGACCTT	GAGTTCCGTCTTGTATTTGGGG	human
Zfp36l1	GATGACCACCACCCTCGT	TGGGAGCACTATAGTTGAGCATC	human
Zfp36l2	CTGCTGCTGACTGCGGTA	ATCCAGACCCACAACTTTGC	human
Rplpo	TCTACAACCCTGAAGTGCTTGAT	CAATCTGCAGACAGACACTGG	human

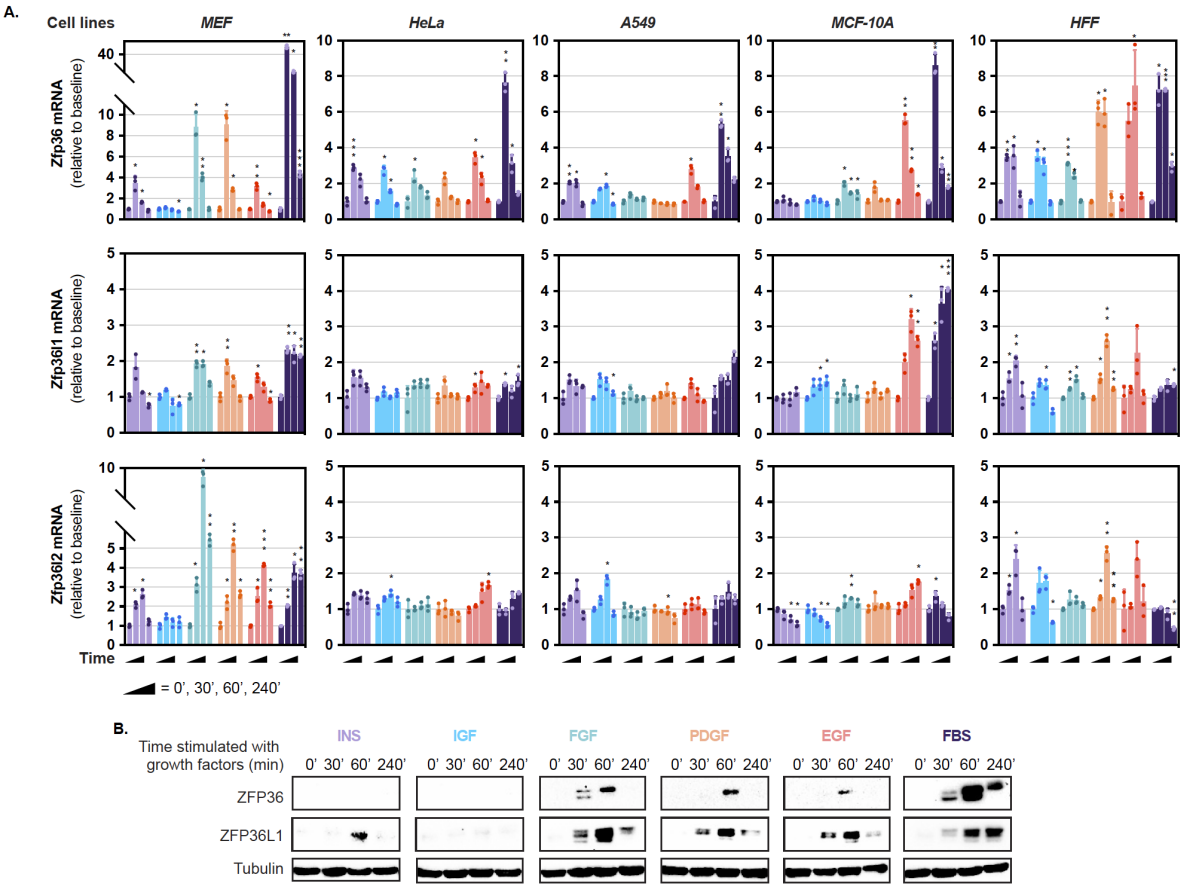

Figure 2-1. Acute growth factor signaling induces ZFP36 family member expression. (A, B) Relative Zfp36/l1/l2 transcript levels (A) or immunoblotting of MEF lysates for ZFP36, ZFP36L1 and tubulin (B) in response to growth factor stimulation (Insulin, 1ug/mL; Igf-1, 100ng/mL; bFGF, 10ng/mL; PDGF-BB, 10ng/mL; EGF, 10ng/mL; or 10% FBS) for 0, 30, 60 or 240-minutes following overnight serum deprivation. Commercially available antibodies for ZFP36L2 are not available for mouse cells, and therefore ZFP36L2 is absent from immunoblotting analyses.

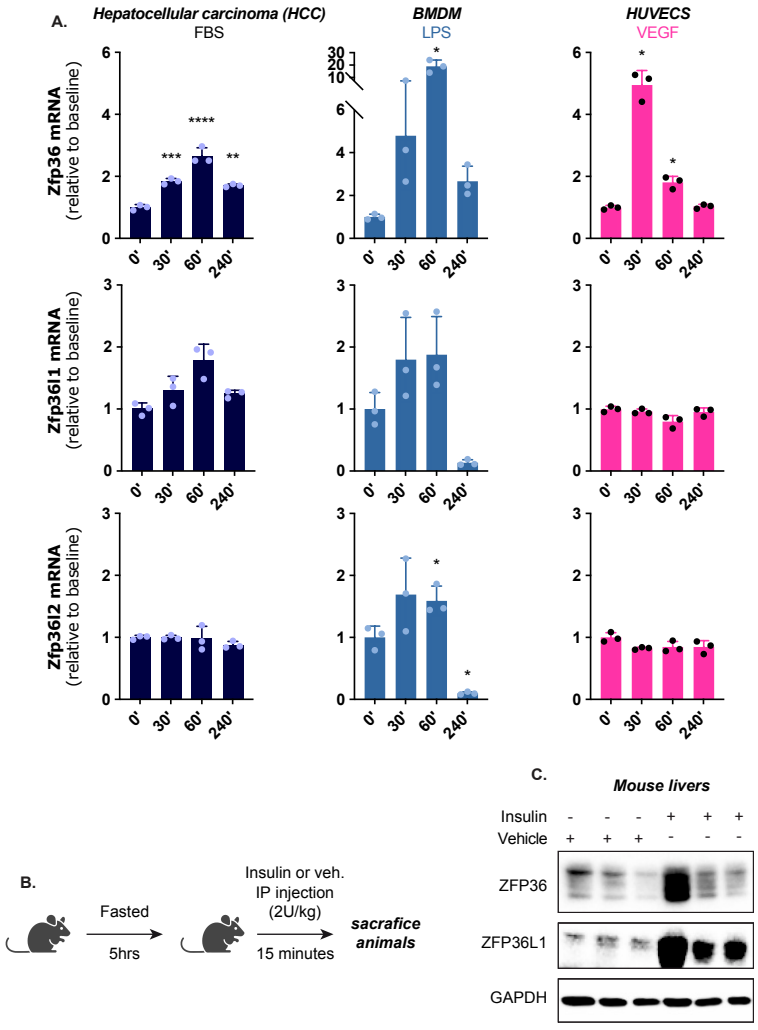

Figure 2-2. ZFP36 family member induction is stimulus- and tissue-specific. Relative Zfp36/l1/l2 transcript levels of hepatocellular carcinoma cells stimulated with 10% FBS, bone marrow-derived macrophages stimulated with LPS, and human umbilical vein endothelial cells stimulated with VEGF. All stimulations were performed for 0, 30, 60 or 240-minutes following overnight serum deprivation. **(B)** Schematic of intraperitoneal (IP) insulin injection for 15 minutes in fasted C57BL/6 mice. **(C)** 15-minute vehicle or insulin-stimulated mouse lysates immunoblotted for ZFP36, ZFP36L1 and GAPDH.

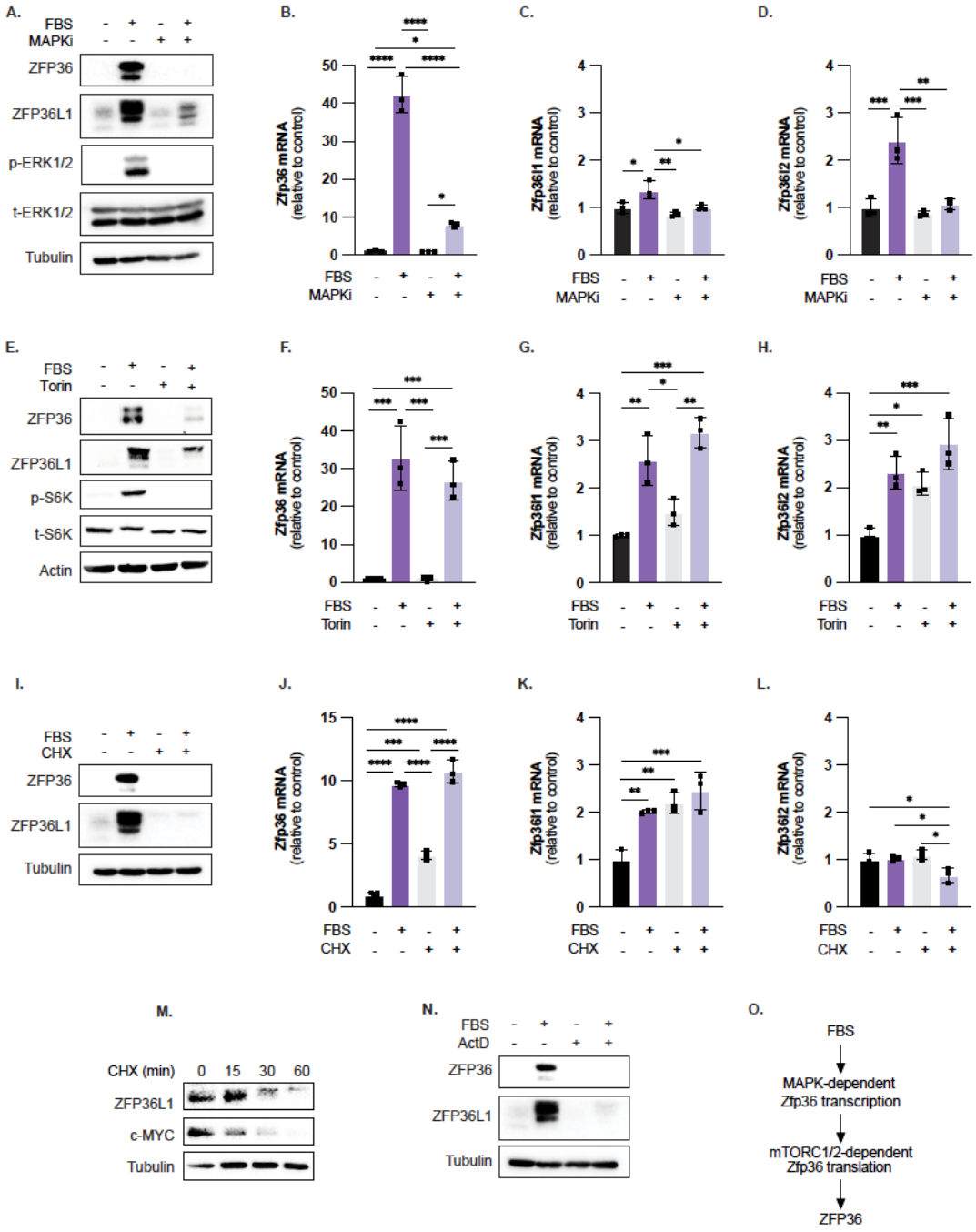

Figure 2-3. ZFP36 proteins are immediate early genes downstream of MAPK and mTORC1/2 signaling. (A) Immunoblot of MEF lysates for ZFP36, ZFP36L1, p42/44 MAPK (total and Thr202/Tyr204), and tubulin. Following overnight serum-deprivation, cells were pretreated for 15-minutes with a small molecule inhibitor cocktail (MAPKi) containing p38 inhibitor SB2035800

(1uM) + Mek1/2 inhibitor PD0325901 (1uM) or DMSO control, +/- 1-hour 10% FBS. **(B-D)** Relative MEF transcript levels of Zfp36 (B), Zfp36l1 (C), and Zfp36l2 (D) +/- 30-minute 10% FBS in the presence or absence of MAPKi pretreatments as described in A. **(E)** Immunoblot of MEF lysates for ZFP36, ZFP36L1, S6K (total and phospho-Thr389) and actin. Cells were serum-deprived overnight and pretreated for 15-minutes with mTORC1/2 inhibitor (Torin, 250nM) or DMSO control, +/- 1 hour 10% FBS. **(F-H)** Relative MEF transcript levels of Zfp36 (F), Zfp36l1 (G), and Zfp36l2 (H) +/- 30-minute 10% FBS in the presence of Torin or DMSO pretreatment as described in (E). **(I)** Immunoblot of MEF lysates for ZFP36, ZFP36L1 and tubulin. Cells were serum-deprived overnight followed by a 15-minute pretreatment with the translation elongation inhibitor cycloheximide (CHX, 100ug/mL) or DMSO control, +/- 1 hour 10% FBS. **(J-L)** Relative MEF transcript levels of Zfp36 (J), Zfp36l1 (K), and Zfp36l2 (L) +/- 30-minute 10% FBS in the presence of CHX or DMSO control as described in I. **(M)** Immunoblot of MEF lysates treated with DMSO or 100mg/mL CHX for 15, 30, or 60-minutes. Lysates were immunoblotted for ZFP36L1, c-MYC and tubulin. Cells were maintained in regular growth medium without being acutely stimulated with serum and therefore lack ZFP36 signal. **(N)** Immunoblot of MEF lysates serum-deprived overnight +/- 1-hour 10% FBS in the presence of the transcription inhibitor actinomycin D (ActD, 5ug/mL) or DMSO control. Lysates were immunoblotted for ZFP36, ZFP36L1, and tubulin. **(O)** Model of acute growth factor signaling-dependent regulation of ZFP36 expression. All experiments were performed with biological replicates. Error bars denote SD (n=3). *p<0.05; **p<0.01; ***p< 0.001.

REFERENCES

1 Cook, D. P. & Vanderhyden, B. C. Context specificity of the EMT transcriptional response. *Nat Commun* **11**, 2142, doi:10.1038/s41467-020-16066-2 (2020).

2 Tang, Y. & Hoffmann, A. Quantifying information of intracellular signaling: progress with machine learning. *Rep Prog Phys* **85**, doi:10.1088/1361-6633/ac7a4a (2022).

3 Dailey, L., Ambrosetti, D., Mansukhani, A. & Basilico, C. Mechanisms underlying differential responses to FGF signaling. *Cytokine Growth Factor Rev* **16**, 233-247, doi:10.1016/j.cytogfr.2005.01.007 (2005).

4 Sen, S., Cheng, Z., Sheu, K. M., Chen, Y. H. & Hoffmann, A. Gene Regulatory Strategies that Decode the Duration of NFkappaB Dynamics Contribute to LPS- versus TNF-Specific Gene Expression. *Cell Syst* **10**, 169-182 e165, doi:10.1016/j.cels.2019.12.004 (2020).

5 Adelaja, A. *et al.* Six distinct NFkappaB signaling codons convey discrete information to distinguish stimuli and enable appropriate macrophage responses. *Immunity* **54**, 916-930 e917, doi:10.1016/j.immuni.2021.04.011 (2021).

6 Amit, I. *et al.* A module of negative feedback regulators defines growth factor signaling. *Nat Genet* **39**, 503-512, doi:10.1038/ng1987 (2007).

7 Mukherjee, N. *et al.* Global target mRNA specification and regulation by the RNA-binding protein ZFP36. *Genome Biol* **15**, R12, doi:10.1186/gb-2014-15-1-r12 (2014).

8 Tiedje, C. *et al.* The RNA-binding protein TTP is a global post-transcriptional regulator of feedback control in inflammation. *Nucleic Acids Res* **44**, 7418-7440, doi:10.1093/nar/gkw474 (2016).

9 Herranz, N. *et al.* mTOR regulates MAPKAPK2 translation to control the senescence-associated secretory phenotype. *Nat Cell Biol* **17**, 1205-1217, doi:10.1038/ncb3225 (2015).

10 Hodson, D. J. *et al.* Deletion of the RNA-binding proteins ZFP36L1 and ZFP36L2 leads to perturbed thymic development and T lymphoblastic leukemia. *Nat Immunol* **11**, 717-724, doi:10.1038/ni.1901 (2010).

11 Vogel, K. U., Bell, L. S., Galloway, A., Ahlfors, H. & Turner, M. The RNA-Binding Proteins Zfp36l1 and Zfp36l2 Enforce the Thymic beta-Selection Checkpoint by Limiting DNA Damage Response Signaling and Cell Cycle Progression. *J Immunol* **197**, 2673-2685, doi:10.4049/jimmunol.1600854 (2016).

12 Rounbehler, R. J. *et al.* Tristetraprolin impairs myc-induced lymphoma and abolishes the malignant state. *Cell* **150**, 563-574, doi:10.1016/j.cell.2012.06.033 (2012).

13 Sawicki, K. T. *et al.* Hepatic tristetraprolin promotes insulin resistance through RNA destabilization of FGF21. *JCI Insight* **3**, doi:10.1172/jci.insight.95948 (2018).

14 Liu, G. Y. & Sabatini, D. M. mTOR at the nexus of nutrition, growth, ageing and disease. *Nat Rev Mol Cell Biol* **21**, 183-203, doi:10.1038/s41580-019-0199-y (2020).

15 Lindqvist, L. M., Tandoc, K., Topisirovic, I. & Furic, L. Cross-talk between protein synthesis, energy metabolism and autophagy in cancer. *Curr Opin Genet Dev* **48**, 104-111, doi:10.1016/j.gde.2017.11.003 (2018).

CHAPTER 3

ZFP36 Regulates Metabolic Gene Expression Through Direct mRNA Decay

INTRODUCTION

Cellular responses to extrinsic cues often require a coordinated change in metabolism. Downstream of growth factor- or cytokine-induced signaling pathway activation, metabolism is regulated at the transcriptional level by transcription factors such as HIF, MYC, and SREBP[1,2]. Metabolism is also regulated at the post-translational level via phosphorylation of metabolic enzymes, such as AKT phosphorylation of ACLY to promote acetyl-CoA production, PANK2/4 to promote CoA synthesis, and NADK to stimulate NADP+ production[3,4,5,6]. However, less is known about how metabolism is regulated post-transcriptionally at the level of mRNA stability. This is notable since the ZFP36 family of mRNA-binding proteins are immediate early genes (Chapter 2) that can quickly alter mRNA stability and thereby impact overall gene expression in response to a stimulus[7-9].

Here, we use enhanced cross-linking immunoprecipitation-sequencing (eCLIP-seq) to show that ZFP36 directly binds many different metabolic genes and nutrient transporters during acute growth factor signaling. We identify AU-rich elements as the top enriched ZFP36 binding motif, which are found within many of the metabolic-related genes bound by ZFP36. We cross-reference our eCLIP-seq dataset with RNA-seq performed in a similar context to identify differentially expressed transcripts directly bound by ZFP36. We rationally choose one metabolic enzyme, Enolase 2, to validate a direct ZFP36-dependent mRNA decay mechanism. Thus, ZFP36 is placed as a direct regulator of metabolic genes in dynamic growth factor signaling cell states.

RESULTS

In order to study the role of ZFP36 induction in growth factor-stimulated cells, we reasoned that ablation of each ZFP36 family member simultaneously would be necessary to observe a functional consequence given their potential redundant and compensatory roles[10,11]. Accordingly, we established immortalized MEFs derived from mice engineered with Lox-P sites flanking each

Zfp36 family member allele. Administration of increasing adenoviral-packaged CRE recombinase (adeno-Cre) or GFP control (adeno-GFP) revealed dose-dependent Zfp36 family member excision within 24-hours post-infection (Figure 3-1A and 3-1B). We optimized adeno-Cre multiplicity of infection (MOI) based on loss of Zfp36, Zfp36l1 and Zfp36l2 mRNA expression (Figure 3-1C) and confirmed loss of ZFP36 and ZFP36L1 protein expression in the adeno-Cre infected FBS-stimulated Zfp36/l1/l2 triple-floxed MEFs (Figure 3-1D). Together these data provide evidence that complete elimination of all ZFP36 family member genes is readily achievable in our Zfp36/l1/l2 triple-floxed MEFs.

eCLIP-seq reveals ZFP36 binding to metabolism-related mRNAs

To unbiasedly identify direct ZFP36-mRNA interactions at the transcriptome-wide level during acute growth factor signaling, we performed enhanced UV cross-linking immunoprecipitation (eCLIP-seq) in biological duplicates. This molecular technique covalently preserves ribonucleoprotein complexes enabling immunoprecipitation of ZFP36 and subsequent sequencing of prepared libraries to determine precise binding site locations at single nucleotide resolution[12]. For these eCLIP-seq experiments, we used Zfp36/l1/l2 triple-floxed MEFs (TFWT) as well as an adeno-Cre-infected Zfp36/l1/l2 triple knockout MEF clone (TFKO.1). TFKO.1 cells controlled for off-target affinities of the ZFP36 antibody. To carryout eCLIP-seq, TFWT and TFKO.1 MEFs were plated in regular growth conditions, serum-starved overnight, then serum-stimulated for 40-minutes to induce ZFP36 protein expression prior to UV cross-linking (Figure 3-2A). Immunoblots of cellular fractions from the TFWT or TFKO.1 MEFs show comparable size-matched input (SMInput) material used for eCLIP-seq normalization, and anti-ZFP36 antibody IgG detection, as well as lack of ZFP36 signal in the TFKO.1-specific lanes (Figure 3-2B). We then excised and sequenced these ZFP36-mRNA complexes, quantitatively scoring each interaction. mRNAs identified in each replicate of the TFKO.1 IP libraries were minimal (≤ 30) and excluded from subsequent analyses (Figure 3-3A and 3-3B). Correlating the score of each eCLIP-

seq duplicate on a gene-by-gene basis revealed highly reproducible (R^2=0.834) results across 3090 commonly bound mRNAs (Figure 3-2C and 3-2D). Impressively, our first eCLIP-seq replicate captured more than 90% of the genes bound by ZFP36 in the second trial. Moreover, the classical categorization of ZFP36 as an RBP that preferentially targets AREs was recapitulated in our hands as indicated by a 5.8-fold enrichment of the UAUUUAUU motif relative to competing binding sites (Figure 3-2E)[13,14]. Our high-confidence binding map of putative ZFP36 target mRNAs also identified known ZFP36 target genes such as Dusp1, Cxcl2, and Ptgs2, which were tiered in the top 25 cross-link scores (Figure 3-2F)[15-18]. Unbiased KEGG pathway enrichment analysis confirmed previously described migratory- and cytokine-related regulatory networks, with proteoglycans in cancer, focal adhesion, and TNF signaling pathways representing the top three unbiased hits (Figure 3-3C)*[18].*

Intriguingly, among known ZFP36 target genes and the cellular processes they participate in, our eCLIP-seq analysis also revealed ZFP36 binding to a large number of mRNAs encoding metabolic enzymes, nutrient transporters and nutrient sensors, which are novel ZFP36 targets (Figure 3-2F-O). This was consistent with MAPK, PI3K-Akt and mTOR KEGG pathway enrichments and further supported by Molecular Function Gene Ontology (GO) terms such as small GTPase binding, Ras GTPase binding and protein serine/threonine kinase activity (Figure 3-3D and 3-3E). Similarly, Biological Processes GO terms revealed positive regulation of cell projection organization and neuron projection development, consistent with regulation of cellular metabolism (Figure 3-3F). We systematically categorized the metabolism-related mRNAs bound by ZFP36 in our eCLIP-seq analysis within common pathways, including glycolysis (Figure 3-2H), oxidative phosphorylation (Figure 3-2I), purine and pyrimidine metabolism (Figure 3-2J-K), fatty acid synthesis (Figure 3-2L), reactive oxygen species (Figure 3-2M), sphingolipid metabolism (Figure 3-2N), and amino acid synthesis (Figure 3-2O). Among the ZFP36-bound mRNAs we identified were those encoding critical regulatory enzymes that likely influence overall pathway

flux. For example, ZFP36 bound to mRNAs encoding key enzymes involved in fatty acid biosynthesis (Fasn), serine synthesis (Phgdh), glutaminolysis (Gls), sphingolipid biosynthesis (Sptlc2), and glycolysis (Hk2, Pfkm, Pkm)[19-24]. Moreover, Slc2a1, the primary glucose transporter in proliferating and cancer cells, was also found bound by ZFP36 (Figure 3-2G). Given the number of bound nutrient transporter mRNAs belonging to the SLC gene superfamily (>40), we presented the top 25 scoring, assigning the bicarbonate transporter Slc4a3 as the top hit, which was recently shown to be limiting for nucleotide synthesis (Figure 3-2G)[25].

To examine whether ZFP36 binding to metabolic transcripts affects metabolic gene expression levels, we used RNA-sequencing in serum-deprived baseline culture conditions or 1-hour post-FBS stimulation – an intentionally delayed time point relative to our eCLIP-seq conditions to allow time for ZFP36-mediated mRNA decay – and examined how levels of ZFP36-bound mRNAs change in the presence versus absence of ZFP36. For this analysis, we profiled mRNA levels from ZFP36/L1/L2 triple-floxed MEFs acutely treated with adeno-Cre (TFKO) or -GFP (TFWT) control for 24-hours (Figure 3-4A). As expected, all three Zfp36 family members were among the most downregulated transcripts in the TFKO cells, and also found bound by ZFP36 in our eCLIP-seq analysis, consistent with their autoregulatory capacity as previously reported (Figure 3-5A)[26]. Conversely, we observed a general overrepresentation of ZFP36-bound mRNAs among the upregulated mRNAs in TFKO cells, consistent with the mRNA decay function of ZFP36 family members (Figure 3-5A). Principal component analysis assigned 5% total expression variance to ZFP36 status, while the remaining 95% was attributed to FBS-dependent changes in gene expression (Figure 3-4B). Importantly, this variance was evident in both serum-deprived and -stimulated conditions suggesting that ZFP36 family member dependencies, although likely distinct in a subset of their constituents, are measurable in the absence of growth factor signaling. This hypothesis was further supported through unbiased hierarchical clustering of significantly differentially expressed genes in serum-deprived or -stimulated conditions, revealing that top

FBS-induced transcripts in TFWT cells become significantly divergent from TFKO cells upon FBS-stimulation; transcripts less responsive to FBS-stimulation appear to exhibit divergence at baseline (Figure 3-4C). Further, given the representation of SLC genes within our eCLIP-seq dataset, we chose to present distinct expression clusters of this gene family, identifying significant upregulation of 4/5 or 3/5 of the highest scoring ZFP36-bound SLC mRNAs in serum-deprived or -stimulated contexts respectively (Figure 3-4D-F). Together, these data support the conclusion that ZFP36 binds to many target transcripts, resulting in a decrease in their relative expression levels.

ZFP36 directly binds and promotes decay of Enolase 2 mRNA

To more closely examine ZFP36 regulation of target mRNAs, we aggregated all upregulated transcripts in each RNA-sequencing condition (TFKO vs TFWT; serum-deprived and -stimulated) that exceeded a $\log_2$ fold change of 1 and a 0.01 p-value threshold. Cross-referencing these genes with our ZFP36 eCLIP-seq list revealed transcripts that are particularly sensitive to ZFP36-mediated mRNA decay, encompassing several known ZFP36 target genes such as Ptgs2, Csf2, and Fgf21 (Figure 3-5B)[15,27,28]. Importantly, these genes span cross-link scores ranging from 13 to 6400 suggesting that expression levels of low and high scoring mRNAs identified in our eCLIP-seq list can be influenced by ZFP36 binding, and are likely a summation of converging regulatory inputs. In support of the hypothesis that ZFP36 regulates metabolic enzymes, we identified the glycolytic enzyme Enolase 2 (Eno2) as among the highest eCLIP-seq-ranked differentially expressed transcripts in our integrated eCLIP- and RNA-seq datasets (Figure 3-5B). To verify a direct relationship between ZFP36 and Eno2, we examined the binding site of ZFP36 within the Eno2 transcript using Integrative Genomics Viewer software. We found that ZFP36 bound Eno2 at a precise location within its 3'UTR characterized by ten overlapping AREs largely conserved in mouse and human (Figure 3-5C and 3-5D). No binding was observed in the TFKO.1 ZFP36/L1/L2

knockout cells, confirming that signal resulted from ZFP36 binding to the Eno2 3'UTR, not from off-target affinities of the ZFP36 antibody used for eCLIP-Seq.

To examine whether ZFP36 impacts Eno2 expression via direct mRNA decay, we single cell-expanded multiple ZFP36/L1/L2 wildtype (TFWT) or knockout (TFKO) clonal MEF cell lines to measure relative Eno2 expression levels and stability. We observed a two- to four-fold increase in Eno2 mRNA in the absence of ZFP36 family members, which is similar in magnitude to expression of known ZFP36 target genes, Ptgs2 and Fgf21 (Figure 3-5E). Notably, Tuba1b, a gene not bound by ZFP36 within our eCLIP-seq dataset or differentially expressed in the RNA-seq, effectively served as a negative control (Figure 3-5E). We found that the increased Eno2 transcript levels in the TFKO MEF clones corresponded to increased ENO2 protein expression (Figure 3-5F). Importantly, expression of ZFP36, but not a zinc-finger mutant ZFP36 deficient in RNA-binding, was sufficient to reduce ENO2 expression in the TFKO cells (Figure 3-5G and 3-5H)[29]. These data suggest direct regulation of Eno2 mRNA expression by ZFP36 RNA binding. To examine whether ZFP36 regulates Eno2 mRNA expression via altering Eno2 mRNA stability, we treated TFWT or TFKO MEF clones with actinomycin D, a pan-transcriptional inhibitor, and compared mRNA levels of Eno2 with that of a known ZFP36 target gene, Fgf21, and a negative control, Tuba1b. We reasoned that in the context of transcription inhibition, changes in mRNA levels would likely be due to changes in mRNA stability. As shown in Figure 3-5I, Eno2 mRNA stability exhibited a striking dependence on the ZFP36 family, comparable to that of Fgf21. However, Tuba1b mRNA levels decreased similarly across all clones tested, providing evidence that mRNA decay was occurring in all conditions, and not dependent on the ZFP36 family. Together, these results suggest that ZFP36 directly regulates ENO2 expression via promoting Eno2 mRNA decay (Figure 3-5J).

DISCUSSION

Here we map ZFP36-RNA interactions in an acute growth factor signaling context. We quantitatively catalogue these interactions on a metabolic pathway-specific basis, identifying nutrient transporters and metabolic enzymes as among the bone fide ZFP36 target gene repertoire. In support of the hypothesis that ZFP36 regulates metabolism through these interactions, we identify key rate-limiting enzymes among the metabolic target genes bound by ZFP36. Given the striking dependence of ENO2 expression on ZFP36-mediated mRNA decay, we predict that overall pathway activity is likely influenced by regulation of these key metabolic mRNAs. Unbiased RNA-seq identified many upregulated mRNAs in the context of acute ZFP36 family member loss suggesting that mRNA decay-mediated regulation can be switched rapidly to change metabolic gene expression. This is consistent with the upregulation of ZFP36 in acute growth factor signaling acting to attenuate induction of inducible mRNAs or downregulate mRNA expression on a rapid timescale of minutes to hours.

By cross-referencing eCLIP-seq with RNA-seq, we assert that we can identify unique mRNAs whose expression relies on direct ZFP36 binding. Our eCLIP-seq binding list contains ZFP36 target genes in an acute growth factor signaling context. Next, we chose to profile the levels of ZFP36-dependent mRNAs using RNA-seq of triple floxed MEFs treated for 24-hours with adenoviral-CRE or GFP control. Here, we believe the differentially expressed transcripts are likely not due to indirect consequences of ZFP36 ablation- a scenario such that the rise in a gene occurs due to transcriptional activity of a ZFP36 target gene, and that rising gene is mistaken as a direct ZFP36 target. Further, since adenoviral infection was controlled for by infecting wildtype cells with adenoviral-GFP, we believe stress responses due to virus infection are similar between conditions; although the extent to which stress-induced transcripts rely on ZFP36-mediated mRNA decay is less clear and perhaps a confounding artifact of the system. Importantly, by cross-referencing eCLIP-seq with RNA-seq – two orthogonal experiments using adenoviral-based acute

vs long-term ZFP36L1/L2 knockout systems – we can minimize artifacts related to our models, identifying true ZFP36 target genes that rise in expression upon loss of ZFP36 decay activity in the presence of growth factor signaling.

MATERIALS AND METHODS

MEF cell line generation

MEF isolation:

To prepare mouse embryonic fibroblasts, embryos were obtained through time mating of Zfp36/l1/l2 triple-floxed males and females. Starting at E0.5, pregnant dams were followed with daily weighing until embryonic day E11.5. The dams were euthanized by cervical dislocation following isoflurane induction. Embryos were removed using sterile dissection practices and rinsed in cold PBS. The fetal heads, spinal columns, and organs were removed and the remaining tissue was processed for cell culture. The tissue was dissociated using a razor blade and TrypLE Express (Fisher Cat. # 12604021) and cells were diluted in complete medium (DMEM containing 15% FBS, 10 mM nonessential amino acids, 4 mM L-glutamate, 1 mM sodium pyruvate, and 1% penicillin/streptomycin). Cells from each embryo were pelleted at 300xg for 5 minutes, resuspended in complete medium, and plated in 10 cm tissue culture dishes. Once cells reached ~80% confluency (24-36hr), each MEF cell line was split 1:5. Several plates were cryopreserved, and the remaining cells were used for immortalization.

MEF immortalization:

Zfp36/l1/l2 triple-floxed MEFs were seeded into 6-well dishes at ~75% confluency. The following day, MEFs were exposed to overnight SV40 transfection using Lipofectamine 3000 Reagent (Fisher Cat# L3000001), then medium was replaced with fresh complete medium for an additional 24-hours. Next, MEFs were serial passaged with varying dilutions ranging between 1:3 and 1:10 to ensure survival while applying selective immortalization pressure. Once MEFs were visibly immortal – assessed by nearly 100% adherent cultures without excessive floating/dead cells (~5-10 passages) – they were cryopreserved in 20% FBS-supplemented complete medium with 5% DMSO.

Cell culture conditions

All cell lines, with the exception of MCF-10A cells and HUVECs, were cultured in DMEM containing 1 mM pyruvate and 4 mM glutamine supplemented with 10% fetal bovine serum (FBS) and 1% penicillin/streptomycin in a humidified incubator at 37°C with 5% CO_2 and atmospheric oxygen; MCF-10A cells were cultured in DMEM/F12 supplemented with 5% horse serum, 10µg/mL insulin, 10µg/mL cholera toxin, 500ng/mL hydrocortisone, and 20ng/mL epidermal growth factor (EGF); HUVECs were cultured in MCDB-131-WOFBS (VEC Technologies) with 10% FBS.

Cell culture treatments

Growth factor stimulation:

10% FBS used in standard culture conditions was re-introduced following overnight FBS-deprived cell cultures at approximately 75-85% cell confluency.

Adenoviral-GFP/CRE infection:

Adenoviral-packaged GFP or CRE (Vector Biolabs) was prepared in DMEM, 2% BSA, and 2.5% glycerol storage buffer at $1x10^{10}$ PFU/mL. Infections were performed by directly spiking adenovirus into culture medium using single-use aliquots.

Adenoviral-GFP/CRE infection:

Adenoviral-packaged GFP or CRE (Vector Biolabs) was prepared in DMEM, 2% BSA, and 2.5% glycerol storage buffer at $1x10^{10}$ PFU/mL. Infections were performed by directly spiking adenovirus into culture medium using single-use aliquots.

Lentivirus production and transduction:

Lentiviral particles were produced in 293T cells by co-transfecting with a construct of interest and third-generation packaging plasmids containing *vsvg*, *gag/pol*, and *rev* sequences. Following a

48-hour incubation, lentivirus-rich medium was filtered through a 0.45□M porous membrane and applied to target cells overnight in the presence of 4 □g/mL polybrene. Next, infected cells were cultured in regular growth medium for 24-hours prior to beginning blasticidin (10□g/mL) antibiotic selection.

ZFP36 eCLIP-sequencing

Cell culture conditions and UV cross-linking:

Zfp36/l1/l2 triple-floxed MEFs (TFWT) or a Zfp36/l1/l2 triple knockout clone (TFKO.1) were seeded subconfluently into 15cm dishes followed by 24-hours serum deprivation. Next, cells were stimulated for 40-minutes with FBS (10% total volume), placed on ice, and washed twice with cold PBS. After aspirating the final PBS wash, 18mL ice cold PBS was added to the culture vessel and cells were UV-irradiated once at 300mJ/cm^2. Cells were scraped into 10mL ice cold PBS, pelleted and snap frozen until use. An eCLIP library replicate was constructed from 12 cross-linked 15-cm plates pooled together and allocated to SMInput or IP; we constructed 8 libraries total, consisting of a SMInput and IP for each cell line in biological duplicate.

Antibody-bead cross-linking preparation:

For each immunoprecipitation, 25μg anti-tristetraprolin antibody (Millipore ABE285) was conjugated to 125ul Protein A Dynabeads (Thermo Fisher) in binding buffer (1mg/mL in PBS) for 1hr at 4°C. Unbound antibody was removed from the beads by two washes with binding buffer. To covalently cross-link antibody to beads, dimethyl pimelimidate (DMP) was dissolved in Wash buffer (0.2 M triethanolamine in PBS) at 13mg/mL immediately prior to use. After a 5-minute wash at 4°C with Wash buffer, DMP was diluted to 0.5X with water and added to the antibody-beads mix at 1:1 ratio for 30-minutes rotating at room temperature. DMP cross-linking was repeated three times then quenched with Quenching buffer (50 mM ethanolamine in PBS) at room

temperature for 5-minutes. Excess antibody (unlinked) was removed using two 5-minute washes with Elution buffer (1 M glycine pH 3), and the remaining antibody-bead complex was rotated overnight at 4°C in CLIP lysis buffer to be used the following day.

Cell lysis, immunoprecipitation and library construction:

UV irradiated cell pellets were processed as previously described by Van Nostrand et al., 2017 in biological duplicate. Briefly, cross-linked cell pellets were lysed with 0.5mL Lysis buffer (50 mM Tris-HCl, 100 mM NaCl, 1% NP-40, 0.1% SDS, 0.5% sodium deoxycholate, 2µg/mL aprotinin, 2µg/mL leupeptin, 0.7µg/mL pepstatin, pH 7.4) for 10 minutes on ice followed by ultrasonication (Bioruptor). 2µl of Turbo DNase (LifeTech) and 5 µl 1:25 diluted RNase I (LifeTech) was added to lysates respectively, then incubated at 37°C for 5 minutes exactly before adding 30µl RNase inhibitor (NEB). Lysates were pelleted and antibody-bead complexes were added to the supernatant followed by 1-hour rocking at 4°C to capture ZFP36-RNA complexes. Next, 2% of total material from each immunoprecipitation was saved as input fractions, while the remaining IP fraction was stringently washed and ligated with 3' barcoded linkers. 20% of the input or IP fractions were then separated by SDS-PAGE and immunoblotted for ZFP36 and GAPDH for evidence of successful processing and to provide a reference for ZFP36-RNA complex excision. The remaining 80% of input or IP fractions was similarly separated by SDS-PAGE and transferred to a nitrocellulose membrane, excising 75kD above the molecular weight of ZFP36 corresponding to approximately 45-120kD. RNA was then released from the membrane with Proteinase K (NEB) and purified with acid-phenol:chloroform, pH 4.5 (with IAA, 125:24:1) (Invitrogen Ambion #AM9722). Samples were concentrated (Zymo) followed by ligation of a 3' liker to SMInput samples. Next, all samples were reverse transcribed and depleted of RNA contamination before ligating a random-mer adapter to the 5' ends. Libraries were quantified by qPCR using primers that anneal to adapter sequences flanking each molecule of RNA. The PCR cycle number for final

eCLIP library amplification was two less than the RT-qPCR Ct values. Replicate libraries were independently sequenced (paired-end; 2x100bp) on the NOVASeq 6000 platform.

eCLIP-seq data processing and analysis:

Reads were processed and aligned to the mouse mm10 genome. UMIs were extracted using umi_tools, adapters were removed with cutadapt, then reads were aligned with STAR and deduplicated with umi_tools[30-32]. Peaks were called with pureclip, using a size-matched input control for each CLIP library[33]. To identify ZFP36-specific peaks, peaks were identified in both the ZFP36/L1/L2 wildtype (TFWT) and triple knockout (TFKO.1) MEF conditions for each library; peaks identified in TFKO.1 libraries were excluded from all downstream TFWT analyses. Motif analysis was performed in a peak-wise manner with Homer[34]. Binding scores were summed across each gene to obtain a per-gene ZFP36 binding score. For gene ontology analysis, genes with a score >0 in both replicates were used with clusterProfiler to find overrepresented categories[35].

Cell lysis and immunoblotting

Cells were lysed in RIPA buffer supplemented with 2µg/mL aprotinin, 2µg/mL leupeptin, 0.7µg/mL pepstatin, 20mM sodium fluoride, 1mM sodium orthovanadate, 1mM dithiothreitol, 10mM beta-glycerophosphate, and 10mM sodium pyrophosphate. Following protein quantification using Bradford reagent, western blots were performed using standard procedures. The following commercially available antibodies were used for immunoblotting: tristetraprolin (Cell Signaling Technology 71632, 1:500), BRF1/2 (Cell Signaling Technology 2119, 1:1000), GAPDH (Cell Signaling Technology 5174, 1:1000), ENO2 (Cell Signaling Technology 9536, 1:1000), and α-tubulin (Sigma T6074, 1:10,000).

Quantitative real-time PCR

Total RNA was isolated from cells using the Qiagen RNeasy Kit followed by on-column DNase digestion and cDNA synthesis using iScript Supermix Kit (Bio-Rad) with 700ng RNA per reaction. Next, cDNA was diluted 5-fold and 2□l was combined with 0.5□M primers in 20□l Power SYBR master mix (Applied Biosystems) and amplified on a QuantStudio5 (Applied Biosystems). Relative transcript levels were calculated using the ΔΔCt method with Rplpo as the reference gene. Table 1 provides primer sequences used.

Quantification and statistical analyses

All experiments were carried out in biological triplicate unless otherwise indicated. We performed a two-way ANOVA with Sidak's multiple comparison test to compare Zfp36/l1/l2 mRNA levels by RT-qPCR in response to growth factor stimulation or inhibitor treatments. Bar graphs depict individual data points compared by a two-tailed Student's t test. All significant results were defined as having a p-value < 0.05. Asterisks indicate the significance of the p-value: $*p < 0.05$; $**p < 0.01$; $***p < 0.001$.

Table 3-1: RT-qPCR primers.

Gene	Forward (5'to 3')	Reverse (5'to 3')	species
Zfp36	AACGGAACTCTGCCACAAGT	AGTGGCATCGAGAGCCATAG	mouse
Zfp36l1	TTCACGACACACCAGATCCT	TGAGCATCTTGTTACCCTTGC	mouse
Zfp36l2	TTCTACGATATCGACTTCTTGTGC	AAGCCCGGAGTGAAGCTC	mouse
Rplpo	CACTGGTCTAGGACCCGAGAAG	GGTGCCTCTGGAGATTTTCG	mouse
Eno2	AGGTAGCAGATCAGGGGAGG	GGATCCCACATCACCAGCAA	mouse
Ptgs2	TGAGTACCGCAAACGCTTCT	CAGCCATTTCCTTCTCTCCTGT	mouse
Fgf21	CCTTGAAGCCAGGGGTCATT	AGGATCAAAGTGAGGCGATCC	mouse
Rplpo	CACTGGTCTAGGACCCGAGAAG	GGTGCCTCTGGAGATTTTCG	mouse

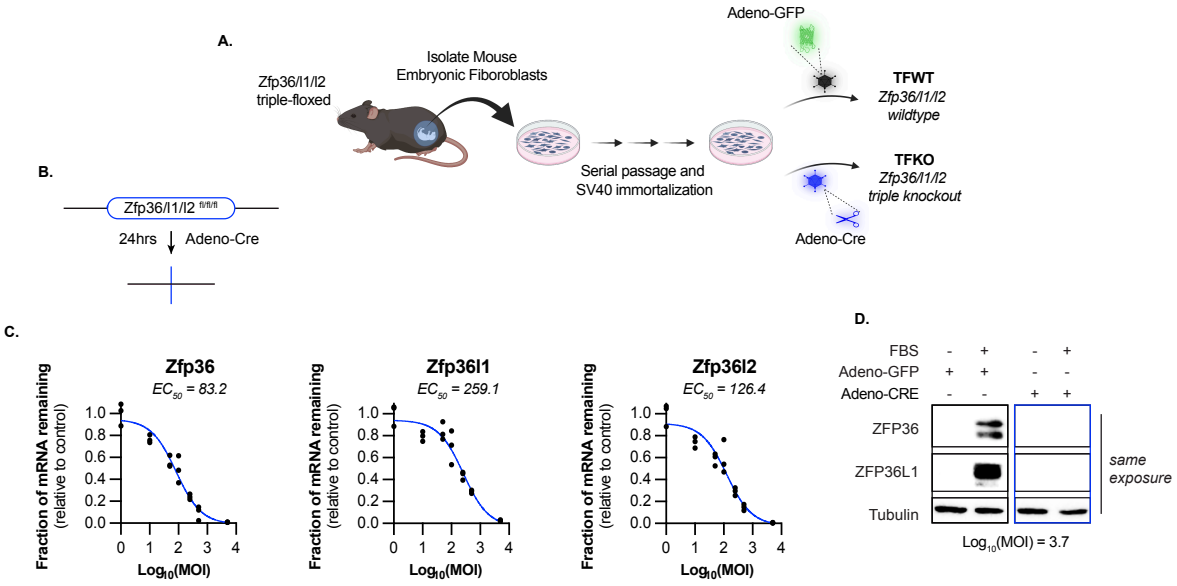

Figure 3-1. ZFP36/L1/L2 triple-floxed MEFs can be excised in vitro with adenovirus-CRE. **(A)** Schematic diagramming Zfp36/l1/l2 triple-floxed MEF cell line generation and adenoviral-based approach for *in vitro* Cre recombinase delivery (adeno-Cre), or GFP control (adeno-GFP), to derive Zfp36/l1/l2 triple-foxed wildtype (TFWT) and triple-floxed knockout (TFKO) cells from an isogenic cell population. **(B)** Schematic diagramming Cre recombinase-mediated recombination of target Lox-P sites flanking both alleles of each of the three ZFP36 family members. **(C)** Relative Zfp36/l1/l2 transcript levels of MEFs pretreated with increasing amounts of adeno-Cre recombinase in serum-free medium for 24-hours, then stimulated with 10% FBS for 30-minutes. Data is fit to an inhibitory EC50 model. **(D)** Immunoblot of triple-floxed MEFs pretreated with Adeno-GFP/CRE (Log_{10}MOI = 3.7) for 24hrs in serum-free medium then stimulated with 10% FBS for 1-hour. Lysates were immunoblotted for ZFP36, ZFP36L1 and tubulin.

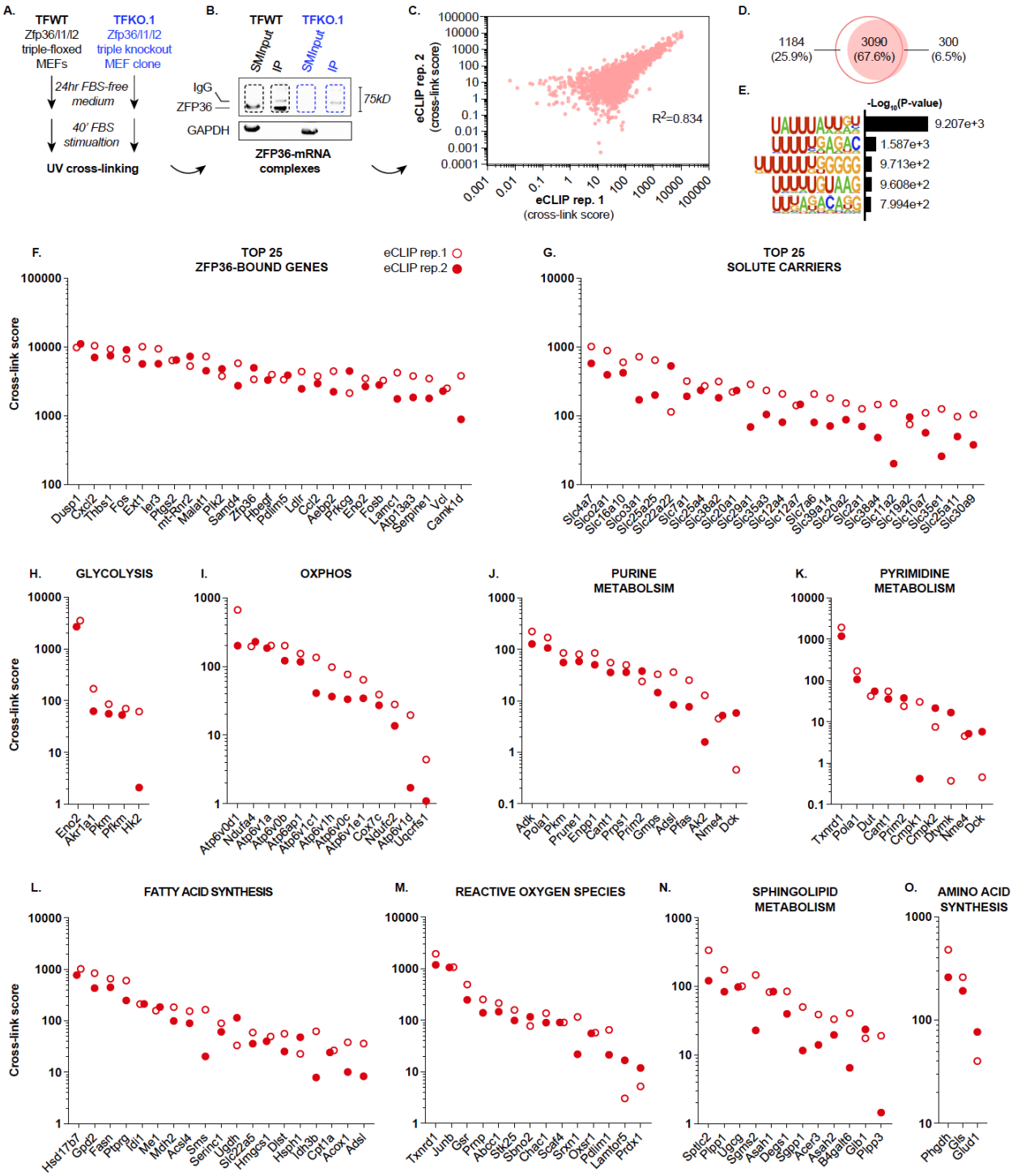

Figure 3-2. eCLIP-seq analysis reveals ZFP36 binding to metabolism-related mRNAs. (A) Schematic diagramming MEF cell lines and culture conditions used for eCLIP-seq library preparation. **(B)** SDS-PAGE immunoblot of UV cross-linked ribonucleoprotein complexes. Input

and ZFP36-immunoprecipitated fractions from ZFP36/L1/L2 wildtype (TFWT) or triple knockout MEF clone (TFKO.1) were immunoblotted for ZFP36 and GAPDH. **(C)** Score correlation per gene between eCLIP-seq replicate 1 & 2. Pearson correlation coefficient shown. **(D)** Overlapping and unique genes from each eCLIP-seq replicate. **(E)** HOMER Motif enrichment analysis of ZFP36 binding sites within target mRNAs identified by eCLIP-seq in both replicates. **(F-O)** High confidence putative ZFP36 target mRNAs identified in both eCLIP-seq ZFP36/L1/L2 wildtype (TFWT) replicates, excluding peaks identified in ZFP36/L1/L2 triple knockout (TFKO.1) replicates, and ranked by UV cross-link score. Data curation was performed using KEGG gene sets from Molecular Signatures Database (MSigDB).

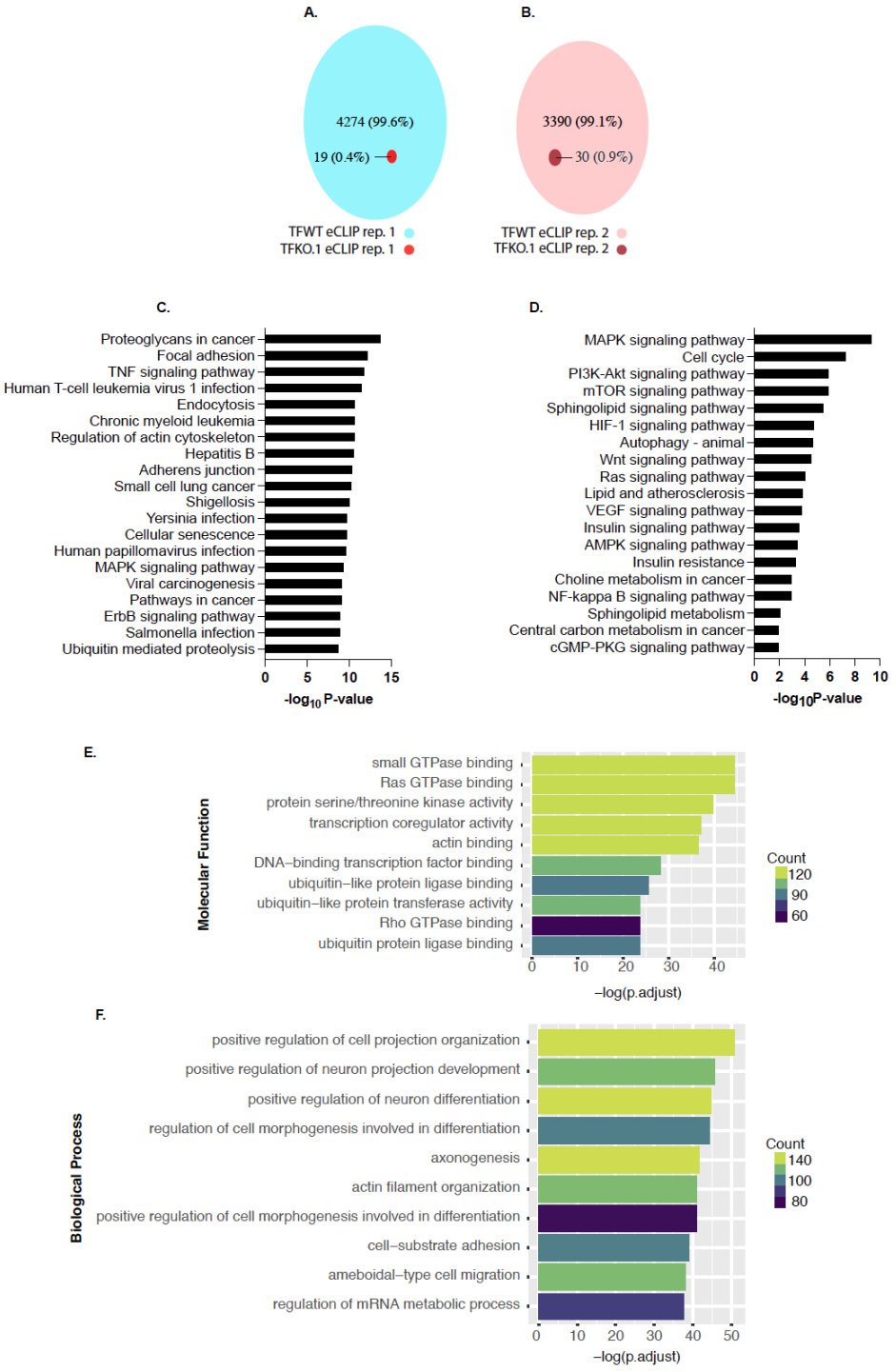

Figure 3-3. ZFP36 eCLIP-seq replicates are highly reproducible revealing known and novel ZFP36 targets. (A, B) eCLIP-seq replicates 1 (A) and 2 (B) depicting number of unique mRNAs bound in ZFP36/L1/L2 wildtype (TFWT) or triple knockout clone (TFKO.1) MEFs. **(C, D)** Unbiased

top 20 (C) or signaling and metabolism-related (D) KEGG pathway overrepresentation. Analysis includes common mRNAs identified in both eCLIP-seq replicates, excluding mRNAs identified in ZFP36/L1/L2 triple knockout (TFKO.1) replicates. **(E, F)** GO Terms: Molecular Function (E) or Biological Process (F) of ZFP36-bound mRNAs identified by eCLIP-seq analysis.

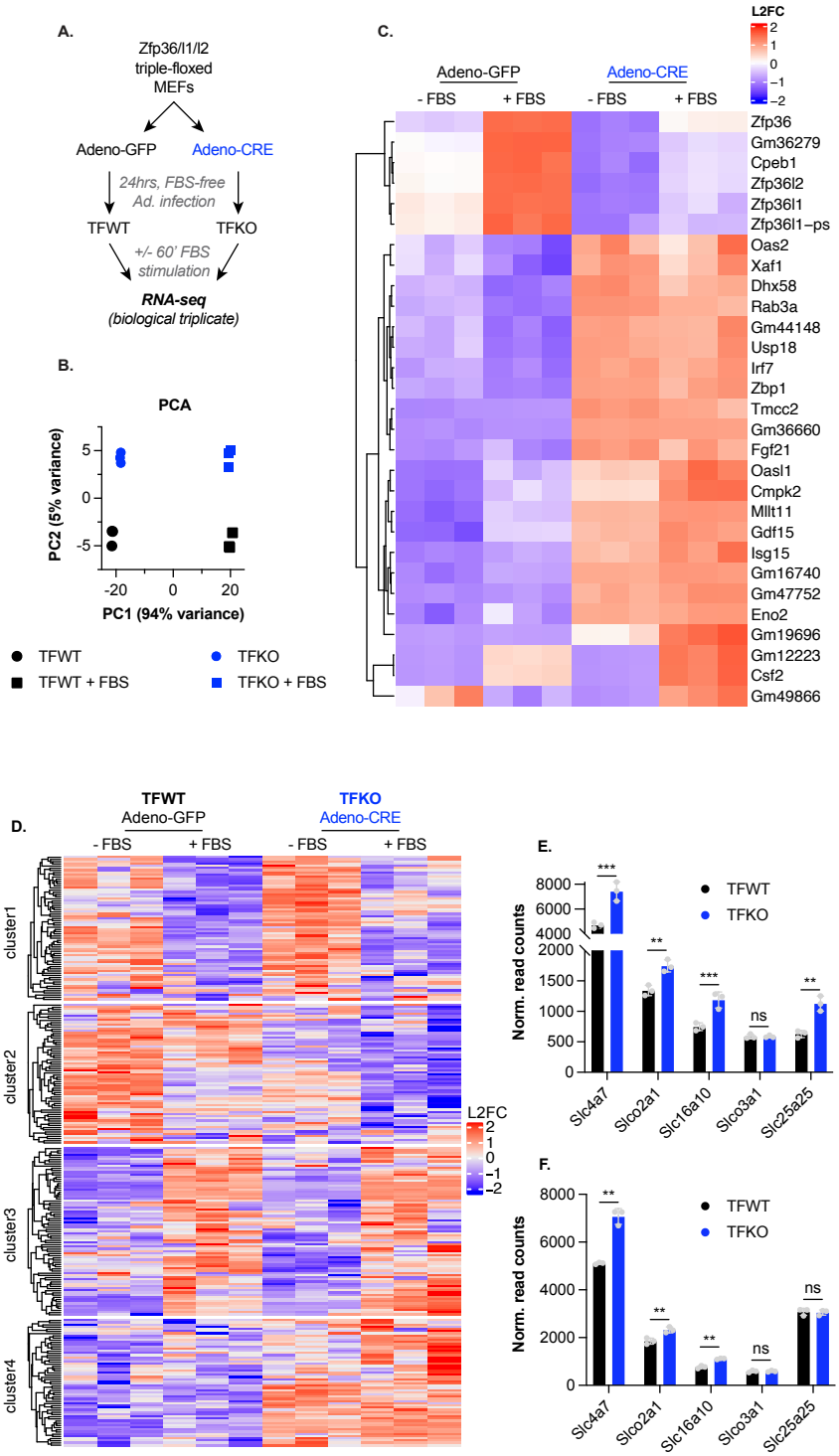

Figure 3-4. RNA-seq identifies ZFP36/L1/L2-dependent gene expression in acute growth factor signaling context. (A) Schematic diagramming adenoviral-based acute Zfp36/l1/l2 family

member gene loss approach for performing RNA-seq. Zfp36/l1/l2 triple-floxed MEFs were exposed to adeno-GFP (TFWT) or adeno-Cre (TFKO) (Log_{10}(MOI) = 3.7) for 24-hours in serum-free medium, +/- one hour 10% FBS stimulation, followed by RNA isolation and sequencing. **(B)** Principal component analysis; PC1 vs PC2 of RNA-seq results for TFWT or TFKO MEFs serum-deprived or 10% FBS-stimulated conditions. **(C)** Unbiased hierarchical clustering of top DEGs (p-value of ≤ 0.01 and a log2(fold-change) of ≥1 or ≤-1), in serum-deprived or -stimulated RNA-seq conditions as described in A. **(D)** Unbiased hierarchical clustering of all solute carrier (SLC) mRNAs from RNA-seq experiment, without applying statistical cut-off filters. **(E, F)** Normalized RNA-seq read counts of top 5 eCLIP-seq scoring ZFP36-bound SLC mRNAs in serum-deprived (E) or serum-stimulated (F) conditions.

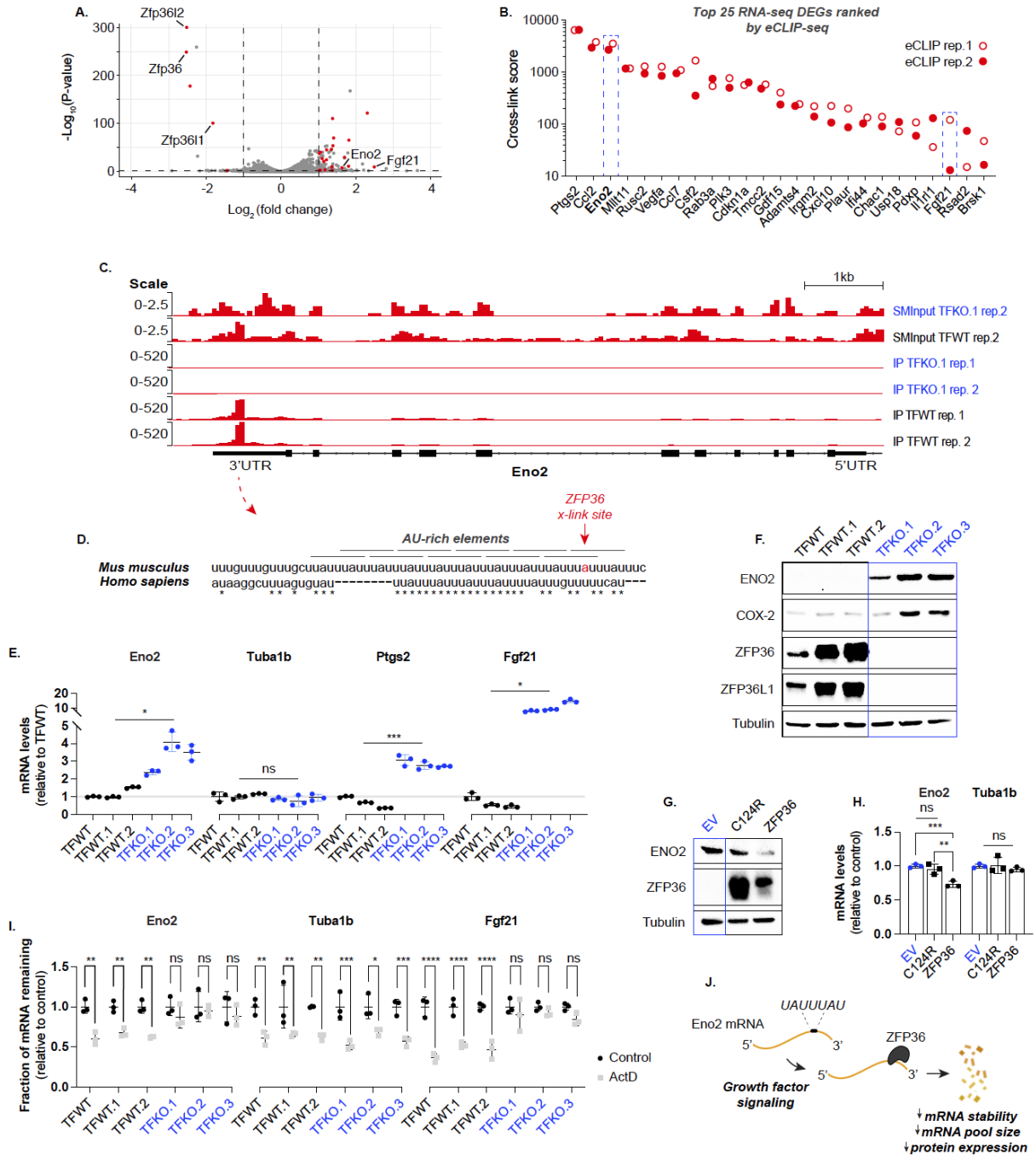

Figure 3-5. ZFP36 directly binds and promotes decay of Eno2 mRNA. (A) RNA-seq volcano plot of adeno-GFP-treated (TFWT) versus adeno-Cre-treated (TFKO) Zfp36/l1/l2 triple floxed MEFs stimulated for 1-hour with 10% FBS following overnight serum deprivation. Dashed lines indicate adjusted p-value ≤ 0.01 or Log_2(fold change) ≥ 1 or ≤ -1. Red colored dots represent

significantly differentially expressed mRNAs also bound by ZFP36 in eCLIP-seq experiment **(B)** Top 25 upregulated transcripts in ZFP36/L1/L2 TKO (TFKO) MEFs identified by RNA-seq from serum-starved and -stimulated culture conditions that are also bound by ZFP36. Genes are ranked by eCLIP-seq cross-link score. **(C)** Integrative Genomics Viewer generated from eCLIP-seq experiments showing the ZFP36 binding site on Eno2 mRNA within 3'UTR. **(D)** Clustal Omega Multiple Sequence Alignment of the ZFP36 target binding sequence within human and mouse Eno2 3'UTRs. AREs are annotated in overlapping gray bars, identities are indicated by asterisks (*), and predominant ZFP36 cross-link site within mouse Eno2 mRNA is colored red. **(E, F)** Relative transcript (E) or protein (F) levels of indicated genes compared between Zfp36/l1/l2 triple-floxed wildtype MEFs (TFWT), and clones derived from TFWT MEFs treated with adeno-GFP (TFWT.1,2) or adeno-Cre (TFKO.1-3) and single cell expanded. **(G-H)** Immunoblot (G) or RT-qPCR (H) of Eno2 or Tuba1b in a ZFP36/L1/L2 triple knockout MEF clone (TFKO.1) transduced with CMV-driven empty vector control (EV), human zinc finger mutant ZFP36 (C124R) or wildtype human ZFP36 (ZFP36). **(I)** Transcript stability of Eno2, Tuba1b or Fgf21 measured by RT-qPCR in MEF cell lines described in E. Cells were deprived of serum for 24-hours then stimulated with 10% FBS for 1-hour (Control) followed by 4-hour actinomycin D (5□g/mL) treatment (ActD). **(J)** Model of direct ZFP36-dependent regulation of Eno2 mRNA downstream of growth factor signaling. All experiments were performed with biological replicates. Error bars denote SD (n=3). *p<0.05; **p<0.01; ***p< 0.001.

REFERENCES

1 Liu, G. Y. & Sabatini, D. M. mTOR at the nexus of nutrition, growth, ageing and disease. *Nat Rev Mol Cell Biol* **21**, 183-203, doi:10.1038/s41580-019-0199-y (2020).

2 Manning, B. D. & Toker, A. AKT/PKB Signaling: Navigating the Network. *Cell* **169**, 381-405, doi:10.1016/j.cell.2017.04.001 (2017).

3 Dibble, C. C. *et al.* PI3K drives the de novo synthesis of coenzyme A from vitamin B5. *Nature* **608**, 192-198, doi:10.1038/s41586-022-04984-8 (2022).

4 Hoxhaj, G. *et al.* Direct stimulation of NADP(+) synthesis through Akt-mediated phosphorylation of NAD kinase. *Science* **363**, 1088-1092, doi:10.1126/science.aau3903 (2019).

5 Covarrubias, A. J. *et al.* Akt-mTORC1 signaling regulates Acly to integrate metabolic input to control of macrophage activation. *Elife* **5**, doi:10.7554/eLife.11612 (2016).

6 Lee, J. V. *et al.* Akt-dependent metabolic reprogramming regulates tumor cell histone acetylation. *Cell Metab* **20**, 306-319, doi:10.1016/j.cmet.2014.06.004 (2014).

7 Amit, I. *et al.* A module of negative feedback regulators defines growth factor signaling. *Nat Genet* **39**, 503-512, doi:10.1038/ng1987 (2007).

8 Kafasla, P., Skliris, A. & Kontoyiannis, D. L. Post-transcriptional coordination of immunological responses by RNA-binding proteins. *Nat Immunol* **15**, 492-502, doi:10.1038/ni.2884 (2014).

9 Hao, S. & Baltimore, D. The stability of mRNA influences the temporal order of the induction of genes encoding inflammatory molecules. *Nat Immunol* **10**, 281-288, doi:10.1038/ni.1699 (2009).

10 Moore, M. J. *et al.* ZFP36 RNA-binding proteins restrain T cell activation and anti-viral immunity. *Elife* **7**, doi:10.7554/eLife.33057 (2018).

11 Cao, J. *et al.* A human cell atlas of fetal gene expression. *Science* **370**, doi:10.1126/science.aba7721 (2020).

12 Van Nostrand, E. L. *et al.* Robust transcriptome-wide discovery of RNA-binding protein binding sites with enhanced CLIP (eCLIP). *Nat Methods* **13**, 508-514, doi:10.1038/nmeth.3810 (2016).

13 Mukherjee, N. *et al.* Global target mRNA specification and regulation by the RNA-binding protein ZFP36. *Genome Biol* **15**, R12, doi:10.1186/gb-2014-15-1-r12 (2014).

14 Brewer, B. Y., Malicka, J., Blackshear, P. J. & Wilson, G. M. RNA sequence elements required for high affinity binding by the zinc finger domain of tristetraprolin: conformational changes coupled to the bipartite nature of Au-rich MRNA-destabilizing motifs. *J Biol Chem* **279**, 27870-27877, doi:10.1074/jbc.M402551200 (2004).

15 Sawaoka, H., Dixon, D. A., Oates, J. A. & Boutaud, O. Tristetraprolin binds to the 3'-untranslated region of cyclooxygenase-2 mRNA. A polyadenylation variant in a cancer cell line lacks the binding site. *J Biol Chem* **278**, 13928-13935, doi:10.1074/jbc.M300016200 (2003).

16 Young, L. E. *et al.* The mRNA binding proteins HuR and tristetraprolin regulate cyclooxygenase 2 expression during colon carcinogenesis. *Gastroenterology* **136**, 1669-1679, doi:10.1053/j.gastro.2009.01.010 (2009).

17 Patial, S. *et al.* Enhanced stability of tristetraprolin mRNA protects mice against immune-mediated inflammatory pathologies. *Proc Natl Acad Sci U S A* **113**, 1865-1870, doi:10.1073/pnas.1519906113 (2016).

18 Tiedje, C. *et al.* The RNA-binding protein TTP is a global post-transcriptional regulator of feedback control in inflammation. *Nucleic Acids Res* **44**, 7418-7440, doi:10.1093/nar/gkw474 (2016).

19 Muthusamy, T. *et al.* Serine restriction alters sphingolipid diversity to constrain tumour growth. *Nature* **586**, 790-795, doi:10.1038/s41586-020-2609-x (2020).

20 Knobloch, M. *et al.* Metabolic control of adult neural stem cell activity by Fasn-dependent lipogenesis. *Nature* **493**, 226-230, doi:10.1038/nature11689 (2013).

21 Yang, M. & Vousden, K. H. Serine and one-carbon metabolism in cancer. *Nat Rev Cancer* **16**, 650-662, doi:10.1038/nrc.2016.81 (2016).

22 Jin, L., Alesi, G. N. & Kang, S. Glutaminolysis as a target for cancer therapy. *Oncogene* **35**, 3619-3625, doi:10.1038/onc.2015.447 (2016).

23 Christofk, H. R., Vander Heiden, M. G., Wu, N., Asara, J. M. & Cantley, L. C. Pyruvate kinase M2 is a phosphotyrosine-binding protein. *Nature* **452**, 181-186, doi:10.1038/nature06667 (2008).

24 Sun, X. *et al.* Discovery and development of tumor glycolysis rate-limiting enzyme inhibitors. *Bioorg Chem* **112**, 104891, doi:10.1016/j.bioorg.2021.104891 (2021).

25 Ali, E. S. *et al.* The mTORC1-SLC4A7 axis stimulates bicarbonate import to enhance de novo nucleotide synthesis. *Mol Cell* **82**, 3284-3298 e3287, doi:10.1016/j.molcel.2022.06.008 (2022).

26 Tchen, C. R., Brook, M., Saklatvala, J. & Clark, A. R. The stability of tristetraprolin mRNA is regulated by mitogen-activated protein kinase p38 and by tristetraprolin itself. *J Biol Chem* **279**, 32393-32400, doi:10.1074/jbc.M402059200 (2004).

27 Tu, Y. *et al.* Tristetraprolin specifically regulates the expression and alternative splicing of immune response genes in HeLa cells. *BMC Immunol* **20**, 13, doi:10.1186/s12865-019-0292-1 (2019).

28 Sawicki, K. T. *et al.* Hepatic tristetraprolin promotes insulin resistance through RNA destabilization of FGF21. *JCI Insight* **3**, doi:10.1172/jci.insight.95948 (2018).

29 Qiu, L. Q., Lai, W. S., Bradbury, A., Zeldin, D. C. & Blackshear, P. J. Tristetraprolin (TTP) coordinately regulates primary and secondary cellular responses to proinflammatory stimuli. *J Leukoc Biol* **97**, 723-736, doi:10.1189/jlb.3A0214-106R (2015).

30 Smith, T., Heger, A. & Sudbery, I. UMI-tools: modeling sequencing errors in Unique Molecular Identifiers to improve quantification accuracy. *Genome Res* **27**, 491-499, doi:10.1101/gr.209601.116 (2017).

31 Martin, M. Cutadapt removes adapter sequences from high-throughput sequencing reads. *EMBnet.journal* **17**, 10-12, doi:10.14806/ej.17.1.200 (2011).

32 Dobin, A. *et al.* STAR: ultrafast universal RNA-seq aligner. *Bioinformatics* **29**, 15-21, doi:10.1093/bioinformatics/bts635 (2013).

33 Krakau, S., Richard, H. & Marsico, A. PureCLIP: capturing target-specific protein-RNA interaction footprints from single-nucleotide CLIP-seq data. *Genome Biol* **18**, 240, doi:10.1186/s13059-017-1364-2 (2017).

34 Heinz, S. *et al.* Simple combinations of lineage-determining transcription factors prime cis-regulatory elements required for macrophage and B cell identities. *Mol Cell* **38**, 576-589, doi:10.1016/j.molcel.2010.05.004 (2010).

35 Yu, G., Wang, L. G., Han, Y. & He, Q. Y. clusterProfiler: an R package for comparing biological themes among gene clusters. *OMICS* **16**, 284-287, doi:10.1089/omi.2011.0118 (2012).

CHAPTER 4

ZFP36 Proteins Regulate Metabolism

INTRODUCTION

Cellular metabolism is tightly regulated and responsive to external stimuli[1]. Similarly, gene expression programs demonstrate a striking dependence on growth signals (Chapter 3), a portion of which serve a metabolic function[2,3]. Therefore, it is rational to integrate these two dynamic cellular processes, linking changes in metabolic enzyme mRNA stability with changes in their enzymatic activity output. Similar approaches are taken with metabolic enzyme post-translational modifications (PTMs), linking signaling activation with enzymatic activity[4-6]. It is argued that this mode of regulation renders cells poised for changes in behavior in the absence of de novo gene expression. However, the extent to which growth factor signaling-induced cell state switches require durable changes in metabolic pathway activity would likely dictate persistence of futile gene expression programs. Moreover, there are likely subsets of metabolic enzymes who predominantly rely on expression levels rather than PTMs to dictate their activity. Given the co-occurrence of ZFP36 family of decay factor expression with growth factor signaling-mediated transcriptomic reprogramming – specifically validated for ENO2 (Chapter 3) – we seek to test the hypothesis that cellular metabolism is influenced through ZFP36-mediated mRNA decay.

Here, we profile the metabolism of a cell transitioning from a resting to growing cell state. We catalogue the metabolite changes at the pathway levels, closely examining glycolysis in lieu of our findings that ZFP36 directly regulates ENO2 expression levels (Chapter 3). We perform kinetic U-^{13}C-glucose tracing to measure accumulation of glycolytic intermediates over time. Strikingly, phosphoenolpyruvate (PEP), the forward reaction product of ENO2, ranked among the most upregulated metabolite in ZFP36/L1/L2 triple knockout MEFs compared to wildtype controls. Further, PEP production is increased in ZFP36/L1/L2/ TKO compared to wildtype MEFs suggesting that enolase enzymatic activity is higher, consistent with elevated ENO2 expression. We conclude that gene expression changes identified in chapter 3 translates to changes in the cellular metabolome perhaps on a gene-specific basis. This assertion is further supported by

examining ENO2 expression *in vivo* in a developmental model of angiogenesis, which toggles the ZFP36/ENO2 axis through VEGF signaling at the angiogenic front. Therefore, we believe mRNA decay-mediated changes in metabolic enzyme expression likely spans various context in developing cells and tissues driven by growth factor signaling.

RESULTS

Given the abundant metabolic mRNAs bound by ZFP36 (Chapter 3; Figure 3-2) and validation that these interactions can lead to changes in expression levels (Chapter 3; Figure 3-5), we next wondered whether ZFP36 impacts cellular metabolism downstream of growth signals. To examine potential regulation of metabolism by ZFP36 family members, we used liquid chromatography-mass spectrometry (LC-MS)-based metabolomics to measure pool sizes of metabolites extracted from FBS-stimulated ZFP36/L1/L2 triple-floxed wildtype (TFWT) or triple knockout (TFKO) MEF clones. Indeed, we observed extensive ZFP36/L1/L2-dependent changes in the cellular metabolome, spanning diverse pathways within central carbon metabolism (Figure 4-1A). Intriguingly, levels of PEP, the forward reaction product of ENO2, are elevated in TFKO cells, consistent with the observed elevation in ENO2 protein expression (Figure 4-1A and Chapter 3; Figure 3-5F). Metabolites from many different pathways were elevated in the context of ZFP36/L1/L2 knockout, consistent with the observed binding of ZFP36 to various nutrient transporters and mRNAs from diverse metabolic pathways. Conversely, the metabolites that exhibited decreased levels in the context of ZFP36/L1/L2 knockout were mainly from specific metabolic pathways involving lipid, nucleotide, and TCA cycle metabolism. We observed downregulation of choline- and ethanolamine-related metabolites as well as specific nucleotide (AIR and GAR) or nucleoside (cytidine) species. Together, these data suggest ZFP36 proteins broadly regulate cellular metabolism in response to acute growth factor signaling.

Next, we examined metabolites altered in ZFP36/L1/L2 knockout MEF clones at the pathway level, comparing all detectable glycolytic intermediates, to gain insight into the specificity of elevated PEP levels. We found that PEP was the most elevated metabolite within glycolysis, with more than a 1.25 log_2 fold change increase (Figure 4-1B). Furthermore, kinetic U-13C-glucose tracing in ZFP36/L1/L2 TFWT versus TFKO.1 MEFs revealed faster accumulation of M+3 PEP in the TFKO.1 cells (Figure 4-1C and 4-1D). These data suggest that ZFP36 family member loss increases cellular activity of enolase, consistent with the observed increase in ENO2 expression in these cells (Chapter3, Figure 3-5F).

ZFP36 regulation of ENO2 expression occurs during retinal angiogenesis in murine neonates

To examine whether ZFP36 regulates Eno2 mRNA expression in response to growth factor signaling in a physiological setting *in vivo*, we evaluated ENO2 levels in a developmental model of retinal angiogenesis where Zfp36 was deleted in the endothelial compartment[7]. We chose to examine potential ENO2 regulation by ZFP36 in endothelial cells *in vivo* since our eCLIP-seq GO term Biological Processes analysis identified various aspects of cell projections and differentiation driven by ZFP36 regulation, which is characteristic of blood vessel-neuron crosstalk during development (Chapter 3; Figure 3-3F)[8,9]. We also identified enrichment of Eno2 in the eye and general discordance between its promoter accessibility (+/- 1Kb TSS) and mRNA expression levels in integrated human fetal single cell ATAC- and RNA-seq datasets (Figure 4-2A and 4-2B)[10,11]. Therefore, we reasoned that developmental processes in retinal tissue specifically may rely on post-transcriptional mechanisms pacing a switch between metabolic activation states. We first confirmed ZFP36 knockout by TdTomato reporter expression, which is a proxy for endothelial cell-specific Zfp36 allele recombination (Figure 4-4A). Indeed, we found increased ENO2 expression in ZFP36 knockout endothelial cells localized specifically at the retina angiogenic front – a region previously described to be rich in VEGF – indicating that ZFP36 regulates ENO2

expression in the angiogenic front *in vivo* (Figure 4-5C-E)[12]. Consistently, we found that cultured HUVECs induce Zfp36 expression in response to VEGF stimulation (Chapter 2; Figure 2-2A). Taken together, these data are consistent with growth factor-dependent induction of ZFP36 in endothelial cells in the developing vasculature impacting metabolic gene expression within retinal tissue.

DISCUSSION

Here, we present post-transcriptional regulation of metabolic gene expression to be a key driver of metabolic reprogramming downstream of growth factor signaling. In ZFP36/L1/L2 triple knockout MEFs, we group changes to metabolite abundance at the pathway level, identifying the forward reaction product of ENO2, PEP, to rank among the most significantly upregulated metabolites within glycolysis and among our ~150 targeted metabolite library, consistent with ZFP36-dependent expression of ENO2 (Chapter 3). Conversely, TCA cycle and lipid-related metabolites were among the only downregulated metabolites. Due to the vast binding of metabolic enzymes and nutrient transporters in the eCLIP-seq dataset, it is perhaps not surprising that many metabolic alterations exist in addition to changes in PEP levels.

Kinetic isotope tracing allowed targeted flux measurements through ENO2 by measuring M+3 PEP isotopomer accumulation[13]. Given that PEP levels reach steady state within several minutes, we measured its accumulation using short (30sec-5min) U13C-glucose tracing timepoints- this was within a linear range of PEP production. Here, we conclude that ZFP36/L1/L2 triple knockout leads to elevated PEP production. Importantly, since ENO2 is not a regulatory step of glycolysis, and also that all regulatory steps of glycolysis (PFK, HK, PK) as well as glucose entry (Glut1/Slc2a1) were bound by ZFP36 in our eCLIP-seq dataset in addition to ENO2, it is possible that ENO2 activity is elevated in a manner that relies on dysregulation of these other glycolytic enzymes[14]. ENO2 activity may only increase as a function of increased substrate availability, and

therefore may similarly be accomplished without the upregulation of ENO2. This alternative hypothesis will require testing of exogenous ENO2 expression in wildtype MEFs to measure its impact on glycolysis and PEP production. Conversely, it would be interesting to test the impact of ENO2 knockout in ZFP36/L1/L2 triple knockout MEFs to identify the remaining metabolic alterations that persist in the absence of ENO2 contributions.

Retinal angiogenesis is a physiological process by which growth factors – mainly VEGF – drive endothelial cell-dependent vessel formation. Here, endothelial cell migration and morphological changes integrate VEGF signaling with spatial specificity[15]. While preserving tissue architecture, we used immunofluorescent microscopy to quantify protein expression of TdTom – a proxy for endothelial cell-specific ZFP36 allele recombination – and ENO2 in CDH5-driven CRE mouse models or littermate controls. We identify regions within the angiogenic front to display dysregulation of ENO2 suggesting that VEGF signaling drives ENO2 degradation by upregulating ZFP36 in this region. Interestingly, as VEGF signaling arises as part of an endothelial cell autocrine loop and is a ZFP36 target gene itself, ZFP36 may behave as a negative regulator of gene expression while also terminating the initial signal input – VEGF[16,17]. Together, these observations place ZFP36 as growth suppressive factor, attempting to maintain homeostasis and resist cell state transitions.

MATERIALS AND METHODS

Intracellular metabolite extraction and mass spectrometry-based metabolomics

Cells were seeded into six-well plates at approximately 75% confluency. For glucose tracing experiments, 10mM U-^{13}C-glucose (Cambridge Isotopes) and 10% dialyzed FBS was substituted for 25 mM D-glucose and 10% FBS respectively. At time of harvest, cells were placed on ice and washed with 150 mM ammonium acetate, pH 7.3, then 500 µL 80% methanol was added to each well and transferred to -80°C for 15 minutes. Cells were then scraped into Eppendorf tubes, vortexed vigorously and centrifuged max speed for 10 minutes at 4°C. 250 µL of supernatant was transferred to a new tube and evaporated under vacuum. Dried metabolites were then stored at -80°C until further processing detailed below.

Dried metabolites were reconstituted in 100 µL of a 50% acetonitrile (ACN) 50% dH20 solution. Samples were vortexed and spun down for 10 min at 17,000g. 70 µL of the supernatant was then transferred to HPLC glass vials. 10 µL of these metabolite solutions were injected per analysis. Samples were run on a Vanquish (Thermo Scientific) UHPLC system with mobile phase A (20mM ammonium carbonate, pH 9.7) and mobile phase B (100% ACN) at a flow rate of 150 µL/min on a SeQuant ZIC-pHILIC Polymeric column (2.1 × 150 mm 5 µm, EMD Millipore) at 35°C. Separation was achieved with a linear gradient from 20% A to 80% A in 20 min followed by a linear gradient from 80% A to 20% A from 20 min to 20.5 min. 20% A was then held from 20.5 min to 28 min. The UHPLC was coupled to a Q-Exactive (Thermo Scientific) mass analyzer running in polarity switching mode with spray-voltage=3.2kV, sheath-gas=40, aux-gas=15, sweep-gas=1, aux-gas-temp=350°C, and capillary-temp=275°C. For both polarities mass scan settings were kept at full-scan-range = (70-1000), ms1-resolution=70,000, max-injection-time=250ms, and AGC-target=1E6. MS2 data was also collected from the top three most abundant singly-charged ions in each scan with normalized-collision-energy=35. Each of the

resulting ".RAW" files was then centroided and converted into two ".mzXML" files (one for positive scans and one for negative scans) using msconvert from ProteoWizard. These ".mzXML" files were imported into the MZmine 2 software package. Ion chromatograms were generated from MS1 spectra via the built-in Automated Data Analysis Pipeline (ADAP) chromatogram module and peaks were detected via the ADAP wavelets algorithm. Peaks were aligned across all samples via the Random sample consensus aligner module, gap-filled, and assigned identities using an exact mass MS1(+/-15ppm) and retention time RT (+/-0.5min) search of our in-house MS1-RT database. Peak boundaries and identifications were then further refined by manual curation. Peaks were quantified by area under the curve integration and exported as CSV files. If stable isotope tracing was used in the experiment, the peak areas were additionally processed via the R package AccuCor 2 to correct for natural isotope abundance. Peak areas for each sample were normalized by the measured area of the internal standard trifluoromethanesulfonate (present in the extraction buffer) and by the number of cells present in the extracted well.

MEF cell line generation

MEF isolation:

To prepare mouse embryonic fibroblasts, embryos were obtained through time mating of Zfp36/l1/l2 triple-floxed males and females. Starting at E0.5, pregnant dams were followed with daily weighing until embryonic day E11.5. The dams were euthanized by cervical dislocation following isoflurane induction. Embryos were removed using sterile dissection practices and rinsed in cold PBS. The fetal heads, spinal columns, and organs were removed and the remaining tissue was processed for cell culture. The tissue was dissociated using a razor blade and TrypLE Express (Fisher Cat. # 12604021) and cells were diluted in complete medium (DMEM containing 15% FBS, 10 mM nonessential amino acids, 4 mM L-glutamate, 1 mM sodium pyruvate, and 1% penicillin/streptomycin). Cells from each embryo were pelleted at 300xg for 5 minutes, resuspended in complete medium, and plated in 10 cm tissue culture dishes. Once cells reached

~80% confluency (24-36hr), each MEF cell line was split 1:5. Several plates were cryopreserved, and the remaining cells were used for immortalization.

MEF immortalization:

Zfp36/l1/l2 triple-floxed MEFs were seeded into 6-well dishes at ~75% confluency. The following day, MEFs were exposed to overnight SV40 transfection using Lipofectamine 3000 Reagent (Fisher Cat# L3000001), then medium was replaced with fresh complete medium for an additional 24-hours. Next, MEFs were serial passaged with varying dilutions ranging between 1:3 and 1:10 to ensure survival while applying selective immortalization pressure. Once MEFs were visibly immortal – assessed by nearly 100% adherent cultures without excessive floating/dead cells (~5-10 passages) – they were cryopreserved in 20% FBS-supplemented complete medium with 5% DMSO.

Clonal MEF cell line generation:

Zfp36/l1/l2 triple-floxed MEFs were seeded into 6-well plates at ~60% confluency then exposed to adeno-CRE or adeno-GFP control (Log_{10}(MOI)=3.4) for 24 hours in complete medium (DMEM 10%FBS). The following day medium was replaced with fresh complete medium for 24 hours then cells were trypsinized and plated into 96-well plates at a density of ~1 cell/well. MEFs were allowed to proliferate for ~7-10 days and monitored for single cell colony outgrowth. Single cell clones were then expanded and screened for ZFP36/L1/L2 gene expression at the RNA and protein level with RT-qPCR and immunoblotting respectively. ZFP36/L1/L2 was confirmed to be absent in adeno-Cre-treated MEFs, while adeno-GFP-treated MEF clones maintained expression of ZFP36/L1/L2 proteins.

Cell culture conditions

MEFs were cultured in DMEM containing 1 mM pyruvate and 4 mM glutamine supplemented with 10% fetal bovine serum (FBS) and 1% penicillin/streptomycin in a humidified incubator at 37°C with 5% CO_2 and atmospheric oxygen.

Cell culture treatments

Growth factor stimulation:

10% FBS was applied directly to overnight FBS-deprived cell cultures at approximately 75-85% cell confluency.

Adenoviral-GFP/CRE infection:

Adenoviral-packaged GFP or CRE (Vector Biolabs) was prepared in DMEM, 2% BSA, and 2.5% glycerol storage buffer at $1x10^{10}$ PFU/mL. Infections were performed by directly spiking adenovirus into culture medium using single-use aliquots.

Analysis of human fetal atlas data

Fetal human single cell ATAC and RNA-seq data of 15 organs was downloaded from DESCARTES[10,11]. Normalized gene expression (TPM) per organ and normalized bigwigs of chromatin accessibility per cell type was used. To summarize chromatin accessibility per tissue, the normalized bigwig score across each promoter (+/-1kb TSS) was summed for each cell type, then the promoter accessibility scores for each gene were averaged across the cell types in each organ. This resulted in a single gene expression and promoter accessibility score for each gene in each of the 15 organs.

Quantification and statistical analyses

All experiments were carried out in biological triplicate unless otherwise indicated. All significant results were defined as having a p-value < 0.05. Asterisks indicate the significance of the p-value: $*p < 0.05$; $**p < 0.01$; $***p < 0.001$.

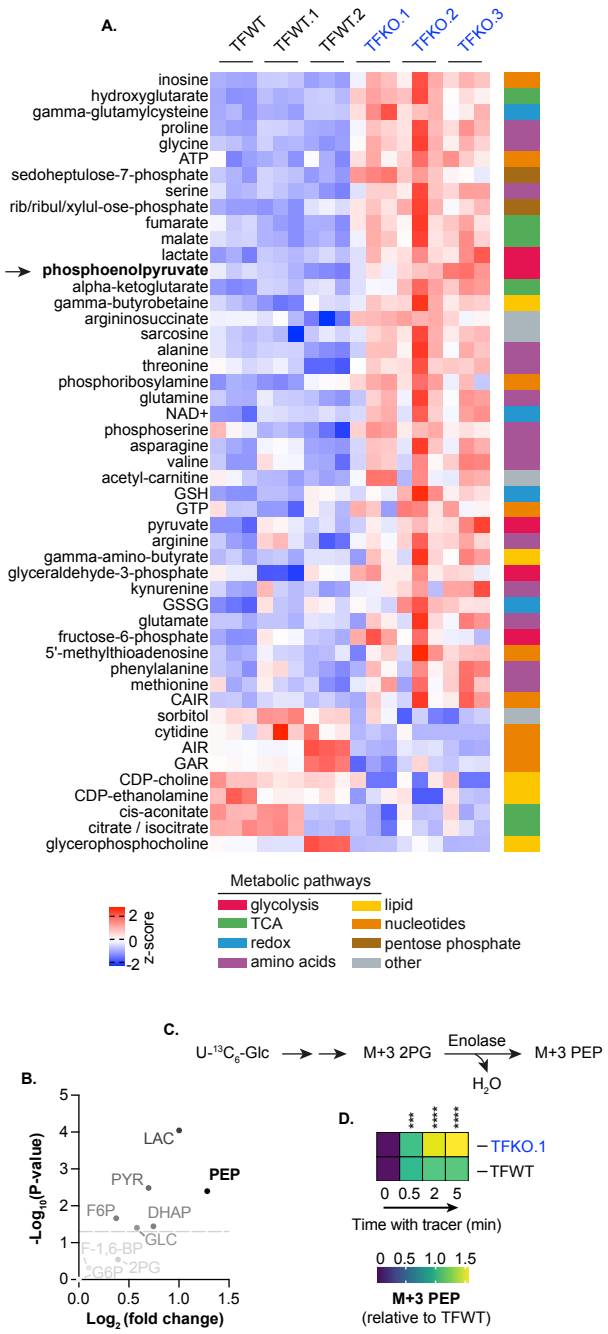

Figure 4-1. ZFP36 proteins regulate cellular metabolism. (A) Targeted LC-MS metabolomics measurements comparing ZFP36/L1/L2 wildtype vs triple knockout clones. Data is grouped by genotype, prefiltered (L2FC ≥ 0.2 or ≤ -0.2; p-value < 0.01) and ranked by statistically significant differential metabolite abundance, then visualized as z-scores across rows. **(B)** Volcano plot comparing glycolytic metabolite levels in ZFP36/L1/L2 triple-floxed knockout MEFs (TFKO.1)

versus Zfp36/l1/l2 triple-floxed wildtype (TFWT) MEFs **(C)** Schematic diagramming uniformly-labeled [13C] glucose tracing through the enolase enzyme and the relevant isotopologues. **(D)** LC-MS measurements of relative levels of U-$13C_6$-glucose-derived M+3 phosphoenolpyruvate (PEP) over time (0, 0.5, 2, or 5-minutes) in Zfp36/l1/l2 triple-floxed wildtype MEFs (TFWT) vs ZFP36/L1/L2 triple-floxed knockout MEFs (TFKO.1) cultured in 10% FBS growth medium. Data are normalized to TFWT cells at 0.5-minute timepoint. All experiments were performed with biological replicates. Error bars denote SD (n=3). *p<0.05; **p<0.01; ***p< 0.001.

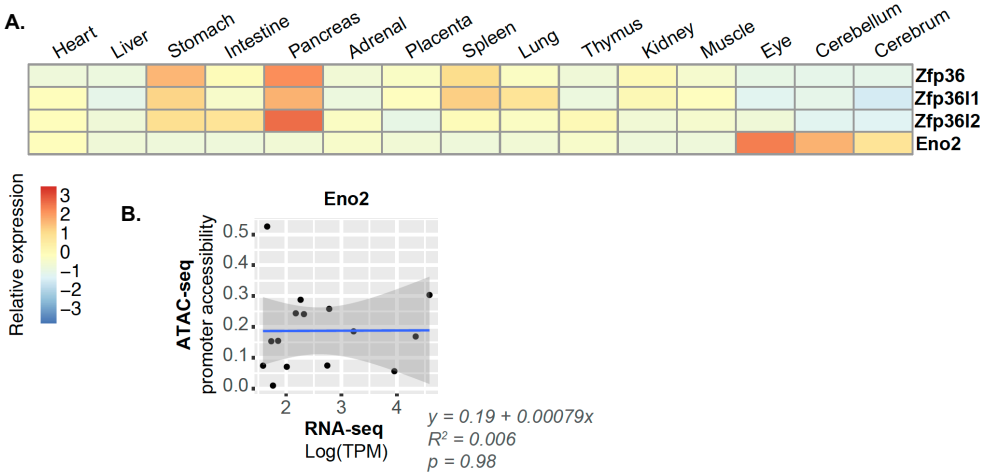

Figure 4-2. Figure 5. ZFP36 regulation of ENO2 expression occurs in human fetal tissues and does not exhibit correlation between promoter accessibility and mRNA expression levels (A) Relative Eno2 expression levels from human fetal single cell RNA-seq atlas across 15 different tissues. **(B)** Correlation of Eno2 expression in single cell RNA-seq and Eno2 ATAC-seq data across human fetal tissues ranging from 89-125 days post-conception.

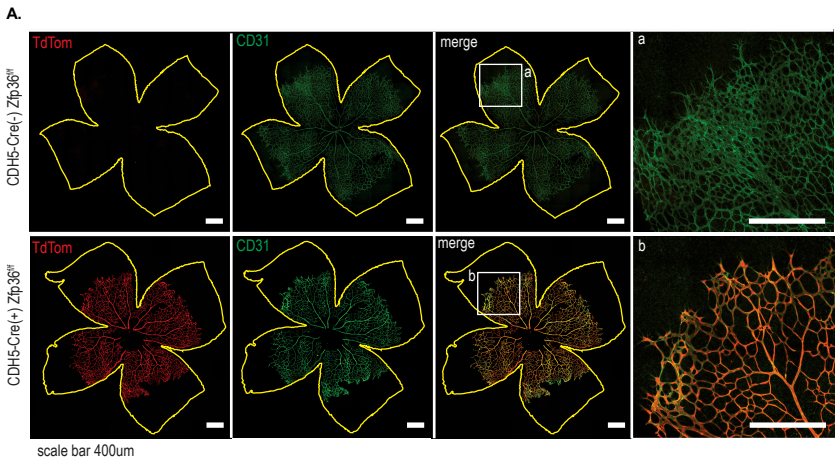

Figure 4-3. TdTomato reporter for CDH5-driven Cre recombination of Zfp36 alleles. (A) Cre(-) or Cre(+) images corresponding to the top or bottom panels respectively. Images depict TdTomato reporter (red) or endothelial-specific CD31 (green).

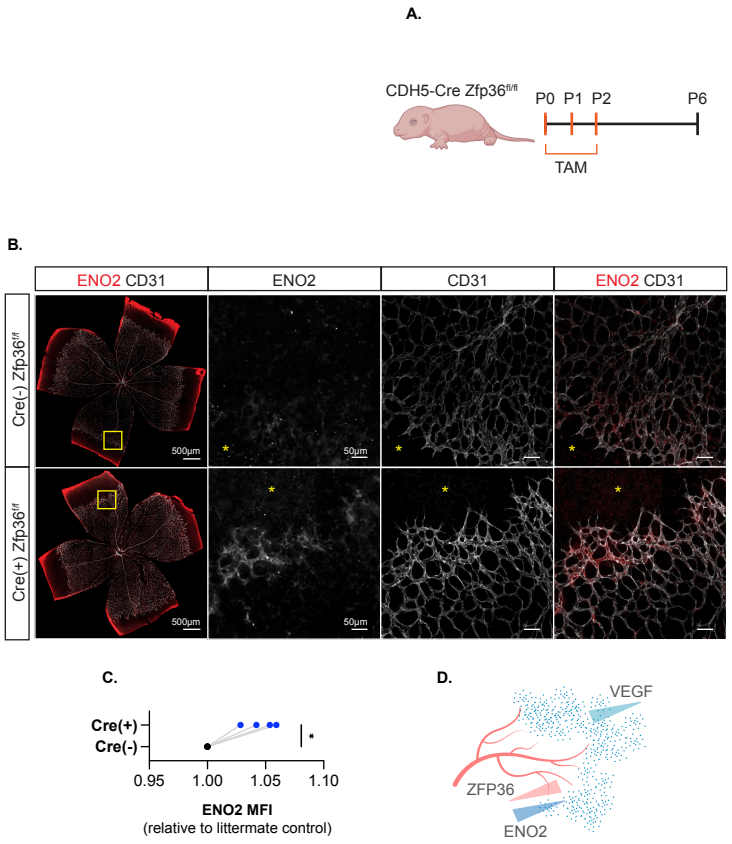

Figure 4-4. ZFP36 regulates Enolase 2 in vivo. (A) Schematic diagramming tamoxifen-inducible (TAM) endothelial-specific Zfp36 knockout in CDH5-Cre Zfp36$^{fl/fl}$ neonatal mice. **(B)** Retina immunostaining of Cre(-) or Cre(+) neonates corresponding to endothelial cell-specific ZFP36 wildtype or knockout respectively. Retinas were stained for endothelial-specific CD31 marker or ENO2. **(C)** Quantification of ENO2 signal comparing Cre(-) and Cre(+) neonatal paired littermates. **(D)** Model of ZFP36 regulation of ENO2 expression downstream of VEGF signaling during retinal angiogenesis in murine neonates.

REFERNCES

1 Mossmann, D., Park, S. & Hall, M. N. mTOR signalling and cellular metabolism are mutual determinants in cancer. *Nat Rev Cancer* **18**, 744-757, doi:10.1038/s41568-018-0074-8 (2018).

2 Byles, V. *et al.* Hepatic mTORC1 signaling activates ATF4 as part of its metabolic response to feeding and insulin. *Mol Metab* **53**, 101309, doi:10.1016/j.molmet.2021.101309 (2021).

3 Torrence, M. E. *et al.* The mTORC1-mediated activation of ATF4 promotes protein and glutathione synthesis downstream of growth signals. *Elife* **10**, doi:10.7554/eLife.63326 (2021).

4 Covarrubias, A. J. *et al.* Akt-mTORC1 signaling regulates Acly to integrate metabolic input to control of macrophage activation. *Elife* **5**, doi:10.7554/eLife.11612 (2016).

5 Dibble, C. C. *et al.* PI3K drives the de novo synthesis of coenzyme A from vitamin B5. *Nature* **608**, 192-198, doi:10.1038/s41586-022-04984-8 (2022).

6 Hoxhaj, G. *et al.* Direct stimulation of NADP(+) synthesis through Akt-mediated phosphorylation of NAD kinase. *Science* **363**, 1088-1092, doi:10.1126/science.aau3903 (2019).

7 Milde, F., Lauw, S., Koumoutsakos, P. & Iruela-Arispe, M. L. The mouse retina in 3D: quantification of vascular growth and remodeling. *Integr Biol (Camb)* **5**, 1426-1438, doi:10.1039/c3ib40085a (2013).

8 Okabe, K. *et al.* Neurons limit angiogenesis by titrating VEGF in retina. *Cell* **159**, 584-596, doi:10.1016/j.cell.2014.09.025 (2014).

9 Cabral, T. *et al.* Retinal and choroidal angiogenesis: a review of new targets. *Int J Retina Vitreous* **3**, 31, doi:10.1186/s40942-017-0084-9 (2017).

10 Cao, J. *et al.* A human cell atlas of fetal gene expression. *Science* **370**, doi:10.1126/science.aba7721 (2020).

11 Domcke, S. *et al.* A human cell atlas of fetal chromatin accessibility. *Science* **370**, doi:10.1126/science.aba7612 (2020).

12 Lundkvist, A., Lee, S., Iruela-Arispe, L., Betsholtz, C. & Gerhardt, H. Growth factor gradients in vascular patterning. *Novartis Found Symp* **283**, 194-201; discussion 201-196, 238-141, doi:10.1002/9780470319413.ch15 (2007).

13 Jang, C., Chen, L. & Rabinowitz, J. D. Metabolomics and Isotope Tracing. *Cell* **173**, 822-837, doi:10.1016/j.cell.2018.03.055 (2018).

14 Zuo, J. *et al.* Glycolysis Rate-Limiting Enzymes: Novel Potential Regulators of Rheumatoid Arthritis Pathogenesis. *Front Immunol* **12**, 779787, doi:10.3389/fimmu.2021.779787 (2021).

15 Gerhardt, H. *et al.* VEGF guides angiogenic sprouting utilizing endothelial tip cell filopodia. *J Cell Biol* **161**, 1163-1177, doi:10.1083/jcb.200302047 (2003).

16 Domigan, C. K. *et al.* Autocrine VEGF maintains endothelial survival through regulation of metabolism and autophagy. *J Cell Sci* **128**, 2236-2248, doi:10.1242/jcs.163774 (2015).

17 Bell, S. E. *et al.* The RNA binding protein Zfp36l1 is required for normal vascularisation and post-transcriptionally regulates VEGF expression. *Dev Dyn* **235**, 3144-3155, doi:10.1002/dvdy.20949 (2006).

CHAPTER 5

Closing Remarks

ZFP36-mediated mRNA decay as a mechanism of rapid metabolic response to growth signals

In this study, we demonstrate rapid upregulation of the ZFP36 family of RNA-binding proteins upon acute growth factor signaling. We provide evidence that ZFP36 directly binds to metabolic enzyme and transporter mRNAs and show that ZFP36 interaction with one bone fide mRNA target, Enolase 2, results in reduced ENO2 expression through a direct mRNA decay mechanism. Finally, we provide evidence that Eno2 is regulated by ZFP36 *in vivo* in a developmental model of VEGF-stimulated retinal angiogenesis. We therefore propose ZFP36-mediated mRNA stability as a critical mode of rapid metabolic regulation downstream of growth factor signaling.

The ZFP36 family of decay factors are fitting players to mediate rapid cell autonomous metabolic reprogramming given their rapid onset of expression within minutes to hours following a growth factor stimulation. Previous evidence recognizes the requirement for ZFP36-mediated regulation of genes within acute and resolving inflammatory contexts, which are known to be facilitated by underlying metabolic transitions. For example, TNFα is the *gold standard* gene shown to be regulated by ZFP36 in LPS-activated macrophages[1]. Later studies expanded the direct ZFP36 binding repertoire to include dozens of inflammatory cytokines across diverse cell lineages. Also found within these datasets are metabolic enzymes whose activities similarly span diverse pathways. Indeed, whole-body knockout mouse models for ZFP36 lead to cachexia, while ablation of all three ZFP36 family members is embryonic lethal – a characteristic of metabolic dysregulation. To our knowledge, our study is the first to directly link ZFP36 to Eno2 mRNA stability [2,3]. We posit that ZFP36-mediated mRNA decay acts on a temporal- and stoichiometric-basis, targeting genes not only with differential affinity – perhaps due to their mere number of AREs – but also within a combinatorial system dictated by relative mRNA expression levels, subcellular localization, existence of secondary mRNA structures or prior occupancy of these

mRNAs by competing RBPs. Metabolic regulation is likely an underappreciated, yet *key*, attribute of ZFP36 function – akin to the upstream signaling pathways that induce ZFP36 expression.

The characterization of metabolites themselves participating in signaling processes has gained more appreciation in recent years[4] . Relevant to the findings presented here, PEP insufficiency culminates in defects in Ca^{2+}-NFAT signaling and cytokine secretory profiles of T cells affecting their anti-tumor effector function[5]. Furthermore, PEP has been postulated as a high-energy phosphate donor, which could account for *some* of its biological function more broadly through mechanisms analogous to ATP[6]. In a separate but potentially related study, prostaglandin (PG) lipid mediators that rely on COX-2 for their synthesis are impinged upon by the cell permeable itaconate derivative, 4-Octyl itaconate (4-OI), to limit their production. 4-OI was shown to decrease Ptgs2/COX-2 mRNA and protein levels independent of NRF2 activity[7]. It is intriguing to speculate that ZFP36 may impact these mechanisms through direct targeting of Eno2 or Ptgs2, as their protein product enzymatic activities produce PEP and PGs respectively.

While our study confirmed ZFP36 regulation of Eno2 mRNA stability and ENO2 expression (Figure 3), we found that ZFP36 directly binds to dozens of transcripts encoding nutrient transporters and metabolic enzymes (Figure 2). Consistently, we found that ZFP36/L1/L2 triple knockout impacts levels of metabolites from diverse metabolic pathways (Figure 4). Together these data suggest that ZFP36 may simultaneously impact many metabolic pathways in response to growth factor signaling, and may serve to broadly coordinate the cellular metabolic response to external stimuli.

ZFP36 proteins participate in a growth suppressive negative feedback module

ZFP36 proteins have been postulated to act as tumor suppressors[8]. A large proportion of ARE-containing transcripts are considered mitogenic, and ZFP36 loss leads to a rise in their

abundance. Interestingly, although we observed ZFP36 family member induction in response to growth factor stimuli within cancer cell lines, the dynamic range of expression was modest relative to normal immortalized cells of similar origin. This finding is consistent with the observation that aged mice decrease ZFP36 compared to their younger counterparts[9]. Moreover, the well-known protooncogene c-Myc transcriptionally represses ZFP36 and is selected for in various malignancies including, but not limited to, B cell lymphomas[10]. We raise the possibility of ZFP36 as a pharmacologic target for stabilization to exploit its pleiotropic affects and inherent biological specificity in various cell growth processes.

Physiological activities during organismal development depend on growth pathways that are also used by cancer cells. Cells must engage in these pathways to contract migratory or proliferative behavior to achieve homeostasis. Regulation occurs with tissue specificity, and the extent to which ZFP36 proteins participate has not been fully elucidated[11,12]. We observe one such biological context – a neonatal murine model of retinal angiogenesis – which exhibits post-transcriptional suppression of ENO2 levels by ZFP36. Previous studies suggest endothelial cells engage glycolysis during angiogenesis[13]. It is not clear the extent to which ZFP36 ablation would promote or inhibit angiogenesis as our observations were limited to identifying the impact of ZFP36 loss on Eno2 gene expression. It is conceivable, however, that endothelial tissue preferentially engages ZFP36-mediated decay to constrain uncontrolled growth. The direct binding of ZFP36 to specific metabolism-related mRNAs, including Eno2, warrants further investigation to uncover the extent to which these interactions result in phenotypic consequences.

ZFP36 proteins are constituents of a broader biological paradigm

This mechanistic link between mRNA decay and rapid metabolic responses – more closely examined for the glycolytic enzyme ENO2 – provides evidence that cells and tissues reserve multiple levels of regulation to accomplish biological outcomes. The rapid onset of ZFP36 family

member-mediated decay in response to growth signals adds an additional facet to a long-standing dogma of transcriptional or post-translational regulatory modules. However, these modes of regulation are clearly not disparate in their action as evident by their role in mediating ZFP36 expression onset through upstream kinases, as well as the numerous phosphorylation sites within ZFP36 proteins themselves that influence their mRNA binding capacity or protein-protein interactions[14]. Since ZFP36 proteins require cooperation with deadenylase complex members to carry out mRNA decay, post-translational modifications on ZFP36 family members are likely central to the broader biological process at play. Our data suggests that cellular metabolism, in addition to being regulated at the transcriptional and post-translational level, is also regulated via the post-transcriptional toggling of mRNA levels, and that rapid cellular metabolic responses to external stimuli are a product of coordinated multi-dimensional regulatory processes.

Limitations of the study

Our study mechanistically dissects ZFP36 binding to metabolic genes and regulation of one metabolic target gene, Eno2, as well as the consequence of this regulation primarily in culture conditions amendable to experimental manipulation. We acknowledge that *in vivo* cellular metabolism is dependent on the surrounding tissue environment, and that *in vitro* cell culture does not recapitulate physiological scenarios. We assert that highly conserved gene regulatory circuits are less dependent on such artifacts, though the extent to which phenotypic outcomes are impacted is less clear. It is this perspective that authenticates the direct ZFP36-mRNA binding interactions revealed by our investigation, warranting further investigation as to the relative *weight* of these relationships to dictate cellular responses on a case-by-case basis. Although we provide evidence that the ZFP36 target gene ENO2 was a predictable relationship generated by our studies, it may not be a universal outcome of ZFP36 loss.

Experimental tools and model systems are often limiting for dissecting biological processes. To this end, we reasoned that ablating all three ZFP36 family members simultaneously would avert redundancy among gene family paralogs and the potential for concluding false negatives in regards to target gene regulation. Indeed, DepMap Portal analyses identify distinct and overlapping co-dependencies for each ZFP36 family member, but the extent to which genetic manipulation of a single family member impacting another has not been fully explored. Further, by employing ZFP36/L1/L2 triple knockout control cells to generate background eCLIP-seq signal, the selective rise ZFP36/L1/L2 target genes may also raise the threshold for identifying true targets. A similar argument can be made for the general over-representation of metabolic enzyme mRNAs within cells. Although eCLIP-seq addresses this technical artifact by normalizing to a SMInput sample – of which we included for each genotype and replicate performed – we nonetheless allow for the possibility that background transcriptome levels influence the signal-to-noise ratio for the eCLIP-seq analytical methodology used in this study.

REFERENCES

1 Carballo, E., Lai, W. S. & Blackshear, P. J. Feedback inhibition of macrophage tumor necrosis factor-alpha production by tristetraprolin. *Science* **281**, 1001-1005, doi:10.1126/science.281.5379.1001 (1998).

2 Dai, W. *et al.* A post-transcriptional mechanism pacing expression of neural genes with precursor cell differentiation status. *Nat Commun* **6**, 7576, doi:10.1038/ncomms8576 (2015).

3 Loh, X. Y. *et al.* RNA-Binding Protein ZFP36L1 Suppresses Hypoxia and Cell-Cycle Signaling. *Cancer Res* **80**, 219-233, doi:10.1158/0008-5472.CAN-18-2796 (2020).

4 Campbell, S. L. & Wellen, K. E. Metabolic Signaling to the Nucleus in Cancer. *Mol Cell* **71**, 398-408, doi:10.1016/j.molcel.2018.07.015 (2018).

5 Ho, P. C. *et al.* Phosphoenolpyruvate Is a Metabolic Checkpoint of Anti-tumor T Cell Responses. *Cell* **162**, 1217-1228, doi:10.1016/j.cell.2015.08.012 (2015).

6 Vander Heiden, M. G. *et al.* Evidence for an alternative glycolytic pathway in rapidly proliferating cells. *Science* **329**, 1492-1499, doi:10.1126/science.1188015 (2010).

7 Diskin, C. *et al.* 4-Octyl-Itaconate and Dimethyl Fumarate Inhibit COX2 Expression and Prostaglandin Production in Macrophages. *J Immunol* **207**, 2561-2569, doi:10.4049/jimmunol.2100488 (2021).

8 Saini, Y., Chen, J. & Patial, S. The Tristetraprolin Family of RNA-Binding Proteins in Cancer: Progress and Future Prospects. *Cancers (Basel)* **12**, doi:10.3390/cancers12061539 (2020).

9 McDonald, A. I. *et al.* Endothelial Regeneration of Large Vessels Is a Biphasic Process Driven by Local Cells with Distinct Proliferative Capacities. *Cell Stem Cell* **23**, 210-225 e216, doi:10.1016/j.stem.2018.07.011 (2018).

10 Rounbehler, R. J. *et al.* Tristetraprolin impairs myc-induced lymphoma and abolishes the malignant state. *Cell* **150**, 563-574, doi:10.1016/j.cell.2012.06.033 (2012).

11 Sullivan, W. J. *et al.* Extracellular Matrix Remodeling Regulates Glucose Metabolism through TXNIP Destabilization. *Cell* **175**, 117-132 e121, doi:10.1016/j.cell.2018.08.017 (2018).

12 Amit, I. *et al.* A module of negative feedback regulators defines growth factor signaling. *Nat Genet* **39**, 503-512, doi:10.1038/ng1987 (2007).

13 Schoors, S. *et al.* Partial and transient reduction of glycolysis by PFKFB3 blockade reduces pathological angiogenesis. *Cell Metab* **19**, 37-48, doi:10.1016/j.cmet.2013.11.008 (2014).

14 Cao, H. *et al.* Identification of the anti-inflammatory protein tristetraprolin as a hyperphosphorylated protein by mass spectrometry and site-directed mutagenesis. *Biochem J* **394**, 285-297, doi:10.1042/BJ20051316 (2006).